Clim Dyn (2015) 44:3449–3468
DOI 10.1007/s00382-014-2165-x

AMOC response to global warming: dependence on the background climate and response timescale

Jiang Zhu · Zhengyu Liu · Jiaxu Zhang · Wei Liu

Received: 20 February 2014 / Accepted: 2 May 2014 / Published online: 14 May 2014
© Springer-Verlag Berlin Heidelberg 2014

Abstract This paper investigates the response of the Atlantic meridional overturning circulation (AMOC) to a sudden doubling of atmospheric CO_2 in the National Center for Atmospheric Research Community Climate System Model version 3, with a focus on differences under different background climates. The findings reveal that the evolution of the AMOC differs significantly between the modern climate and the last glacial maximum (LGM). In the modern climate, the AMOC decreases (by 25 %, 4 Sv) in the first 100 years and then recovers slowly (by 6 %, 1 Sv) by the end of the 1,500-year simulation. At the LGM, the AMOC also weakens (by 8 %, 1 Sv) in the initial 90 years, but then recovers, first rapidly (by 30 %, 4 Sv) over the following 300 years, and then slowly (by 13 %, 1.6 Sv) during the remainder of the integration. These results suggest that the responses of the AMOC under both climates have a similar initial rapid weakening period of ~100 years and a final slow strengthening period over 1,000 years long. However, additional intermediate period of ~300 years does occur for the LGM, with rapid intensification in the AMOC. Analyses suggest that the rapid intensification is triggered and sustained primarily by a coupled sea ice–ocean feedback: the reduction of meltwater flux in the northern North Atlantic—associated with the remarkable sea-ice retreat at the LGM—intensifies the AMOC and northward heat transport, which, in turn, causes further sea-ice retreat and more reduction of meltwater. These processes are insignificant under modern conditions.

Keywords Atlantic meridional overturning circulation · Carbon dioxide · Last glacial maximum · Sea ice · Timescale

1 Introduction

Transporting large amounts of heat, freshwater and nutrients, the Atlantic meridional overturning circulation (AMOC) is an essential component of the climate system (Ganachaud and Wunsch 2000). The AMOC could vary significantly in response to global climate change and variations in atmospheric CO_2. For example, both paleoclimate proxy records (McManus et al. 2004; Robinson et al. 2005) and climate model simulations (Liu et al. 2009) indicate that the AMOC has undergone significant variations during the last deglaciation (20–6 ka before A.D. 1950) when atmospheric CO_2 increased from 185 to 265 ppmv. For future responses to global warming caused by the anthropogenic CO_2 emission, one robust feature across almost all climate models is a weakening of the AMOC over the next ~100 years (Schmittner et al. 2005; Weaver et al. 2012).

However, the relationship between the strength of the AMOC and atmospheric CO_2 concentration could be complicated (Toggweiler and Russell 2008): global warming and CO_2 increase could either strengthen or

J. Zhu (✉) · Z. Liu (✉) · J. Zhang
Department of Atmospheric and Oceanic Sciences and Center for Climatic Research, University of Wisconsin-Madison, 1225 W. Dayton St., Madison, WI 53706, USA
e-mail: jzhu47@wisc.edu

Z. Liu
e-mail: zliu3@wisc.edu

Z. Liu
Laboratory for Climate and Ocean-Atmosphere Studies, School of Physics, Peking University, Beijing 100871, People's Republic of China

W. Liu
Scripps Institution of Oceanography, University of California, San Diego, La Jolla, CA 92093, USA

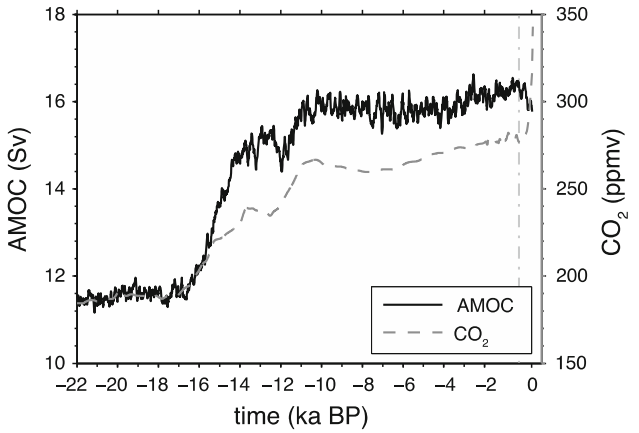

Fig. 1 The evolution of the maximum AMOC in the TraCE-GHG single forcing simulation (*left axis*) and the corresponding variations of atmospheric CO_2 concentration (*right axis*) over the past 22 ka. Note that the last 200 years are elongated by a factor of two for illustrative purpose

weaken the AMOC. The weaker AMOC at the last glacial maximum (LGM, 22–19 ka) implied by proxy records (Duplessy et al. 1988; Lynch-Stieglitz et al. 2007), suggests that the deglacial global warming could produce a stronger AMOC, contrary to the projected weakening to the anthropogenic global warming. This complex relationship is captured by a recent transient simulation (TraCE-GHG, He et al. 2013), which is forced by transient variations in the greenhouse gases (GHGs) concentrations over the past 22 ka with otherwise the same boundary conditions as at the LGM (Liu et al. 2009; He 2011). In TraCE-GHG, the AMOC intensifies by 40 % (4.5 Sv) in response to the 40 % (70 ppmv) deglacial increase of CO_2 at the LGM (Fig. 1), which is consistent with paleo-records showing that the modern climate with higher CO_2 has a stronger AMOC. Furthermore, a closer inspection of the AMOC evolution in the last 150 years of the simulation shows a decreased AMOC in response to the rapid rise of anthropogenic GHGs, which is consistent with the Intergovernmental Panel on Climate Change (IPCC) projections. Both the background climate states and the timescales of the forcing and response are different in this transient simulation. Therefore, it is still an open question that whether the complicated responses of the AMOC to the global warming and CO_2 increase are caused by the different background climates or the response timescales.

In addition to the complicated responses of the AMOC to CO_2 variations, the controlling mechanisms are also open to debate. Southern control processes for the weaker glacial AMOC have been proposed by several previous modelling studies (Shin et al. 2003a, b; Liu et al. 2005): the enhanced sea-ice expansion in the Southern Ocean associated with the glaciation CO_2 decrease leads to increased brine rejection, intensified Antarctic Bottom Water (AABW) formation, and eventually a weaker glacial AMOC. However, many other modelling studies show yet different mechanisms in controlling the intensification of the AMOC to atmospheric CO_2 increase or warming (Saenko et al. 2004; Knorr and Lohmann 2007; Banderas et al. 2012; Oka et al. 2012). These studies suggest a dominating contribution from the North Atlantic (northern control processes), albeit with some difference in the details: some emphasize the changes in freshwater flux (Saenko et al. 2004), some highlight the sea-ice insulating effect and the resultant changes in the atmospheric heat loss (Banderas et al. 2012; Oka et al. 2012), while others stress the subsurface warming and the salt transport processes (Knorr and Lohmann 2007).

These seeming contradictory results of the AMOC response to the increase of CO_2 raise important questions: are the different AMOC responses produced by the differences in the background states (glacial vs. modern) or timescales, and what are the underlying physical mechanisms? This paper is an attempt to understand these questions. We will perform sensitivity experiments to examine the responses of the AMOC to an increased CO_2 forcing in two realistic background climates, the LGM and the modern climate. Furthermore, we will study the entire evolution of the AMOC changes, including the initial, intermediate and final equilibrium responses. This analysis will help illustrate the mechanisms underlying the AMOC response at different timescales. Our findings reveal that responses of the AMOC under these two climates are very distinct and involve different timescales. The analyses on surface density flux suggest that changes in the surface heat flux are important for the short-term response of the AMOC in both climates. By further diagnosing the density changes in the Atlantic Ocean, we find that the coupled sea ice–ocean feedback between the AMOC and the meltwater flux at the LGM causes the major difference from the modern climate at longer timescales. The remainder of this paper is arranged as follows. Section 2 provides a brief description of the model and experiments. The responses of the AMOC to a sudden doubling of CO_2 under the modern and glacial climate states are compared in Sect. 3. We then investigate the mechanisms underlying the AMOC responses by analysing changes in the surface density flux in Sect. 4, and changes in the subsurface density in Sect. 5. A summary and further discussions are given in Sect. 6.

2 Model and experiments

We conducted a set of numerical experiments using a global coupled ocean–atmosphere–land–sea-ice General Circulation Model (GCM), the National Center for Atmospheric Research Community Climate System Model

Table 1 Comparisons of the modern control and LGM control experiments

Exp. name	CO_2 (ppmv)	Orbital and ice sheet (ka)	Surface temperature (°C)	Max. AMOC (Sv)	Sea-ice coverage in subpolar N. Atlantic (40°–80°N) (%)	Equilibrium climate sensitivity (°C)
MOD	355	0	14.04 (0.08)	15.4 (1.06)	22	2.25 (0.8)
LGM	185	22	7.67 (0.09)	12.7 (0.77)	51	3.44 (0.9)

The standard deviations of some variables are in parentheses

version 3 (NCAR CCSM3) (Yeager et al. 2006). The model consists of a primitive equation atmospheric model at T31 horizontal resolution with 26 sigma levels, a land surface model at T31 resolution, a primitive equation ocean model at a nominal 3-degree horizontal resolution with 25 vertical levels. The modern control simulation (MOD, hereafter) has been integrated for more than 1,000 model years and reached equilibrium for the upper ocean and the AMOC, as well as the Southern Ocean processes (Yeager et al. 2006). In this study, MOD is further integrated for 800 model years, and the deep ocean has also reached quasi-equilibrium with a very small drift in global mean ocean temperature of 0.002 °C century^{-1} (vs 0.01 °C century^{-1} in Yeager et al. 2006). The LGM control simulation (LGM, hereafter) is branched from a transient simulation of the last 21,000 years (Liu et al. 2009; He 2011), starting from 22 ka before present. LGM is then integrated further for 1,500 years, and the drift in global mean ocean temperature is even smaller at approximately 0.0003 °C century^{-1}. The climatic forcings used in the control experiments are listed in Table 1. The concentration of atmospheric CO_2 at the LGM is set for the glacial value of 185 ppmv, while it is the modern value of 355 ppmv in MOD. The solar insolation and other GHGs for the LGM are also adjusted to the value at 22 ka. The ocean bathymetry, continental topography and albedo are modified according to the ICE-5G reconstruction (Peltier 2004). Parallel to these two control runs, we carried out two sensitivity experiments, in which the atmospheric CO_2 is doubled instantaneously to 370 and 710 ppmv for the modern climate and the LGM (MOD-2CO2 and LGM-2CO2, hereafter), respectively. All other climatic factors are prescribed at the same values as their control simulations. Each sensitivity experiment is integrated for 1,500 model years with the climate reaching quasi-equilibrium. The response is defined as the difference in MOD-2CO2 and LGM-2CO2 from the mean state of their corresponding control simulations.

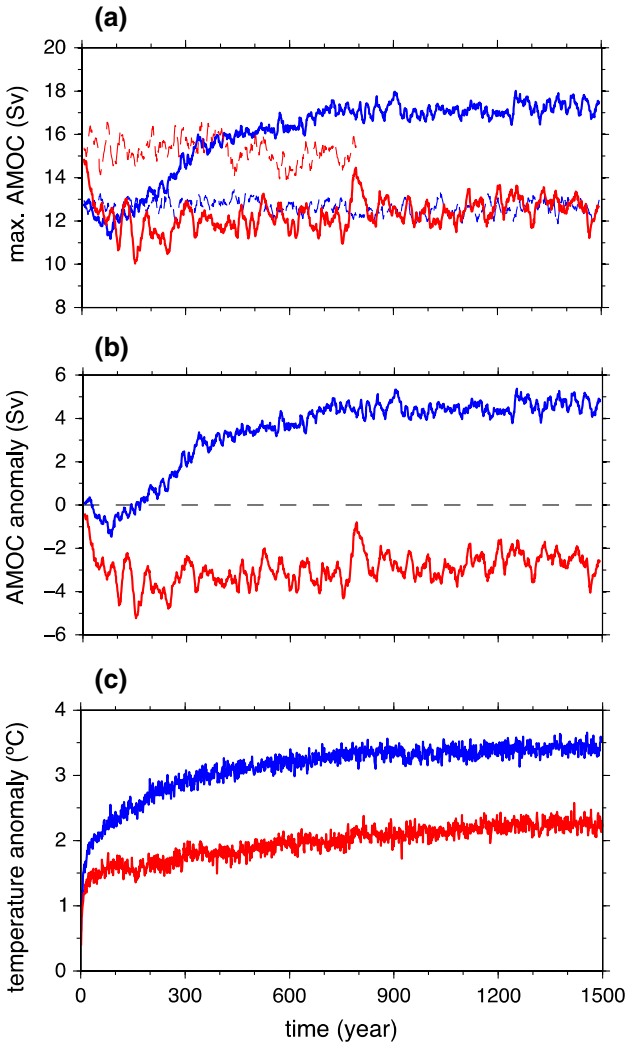

Fig. 2 **a** The evolution of the maximum AMOC in the control simulations (*dashed*) and doubling CO_2 experiments (*solid*) for the modern climate (*red*) and LGM (*blue*). **b** The response of the AMOC in the doubling CO_2 experiments for the modern climate (*red*) and LGM (*blue*). **c** same as **b**, but for the annual-mean global surface temperature

3 Different responses of the AMOC at the modern and LGM climates

The global annual mean surface temperature increases very rapidly in response to the doubling of atmospheric CO_2, as demonstrated in Fig. 2c. The equilibrium climate sensitivity (ECS, the average response in the last 100 years) in MOD-2CO2 and LGM-2CO2 is 2.25 and 3.44 °C with the interannual standard deviation of 0.08 and 0.09 °C (Table 1), respectively. The ECS of the modern climate in this work is slightly smaller than the value of 2.46 ± 0.9 °C in a previous study (Danabasoglu and Gent

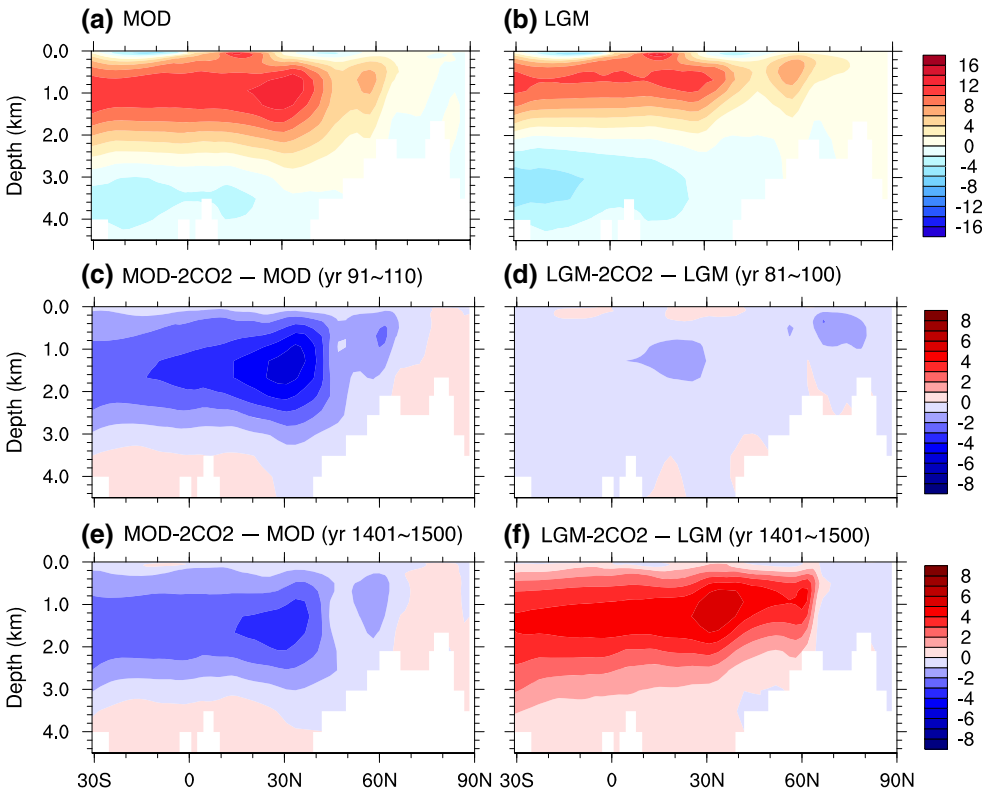

Fig. 3 The streamfunction of meridional overturning in the Atlantic Ocean in the control simulations for the modern climate (**a**) and LGM (**b**), the difference in doubling CO_2 experiments at the year 100 for the modern climate (**c**) and the year 90 for LGM (**d**), and the final quasi-equilibrium response (difference of the last 100 model years from the control simulations) in the doubling CO_2 experiments for the modern climate (**e**) and LGM (**f**). The contour intervals are 2 and 1 Sv for the control and doubling CO_2 experiments, respectively

2009) using the same model but with an integration length of 3,000 years. This indicates that our experiments have reached quasi-equilibrium for the surface climate, although only with 1,500 model years. The ECS of the LGM is markedly larger than that of the modern climate, likely owing to the greater sea-ice coverage during the glacial period (Kutzbach et al. 2013).

The model AMOC in MOD is very stable and has a maximum strength of 15.4 Sv (Table 1; Fig. 2a, red dashed line), marginally weaker than the observational estimation of 18 Sv (Talley et al. 2003). At the LGM, the AMOC and the associated NADW is shallower while the AABW is stronger and expands further northward (Fig. 3a, b), all of which is consistent with the proxy records (Duplessy et al. 1988; Lynch-Stieglitz et al. 2007). The LGM AMOC has an overturning transport that is 18 % weaker than MOD (Table 1; Fig. 2a, blue dashed line). These differences between MOD and LGM could be attributable to the different sea-ice configurations (Shin et al. 2003a; Otto-Bliesner et al. 2007).

The response of the AMOC to the doubling of atmospheric CO_2 depends significantly on background climates. For the modern climate, in MOD-2CO2, the AMOC decreases by 25 % in the first 100 years from 15.4 to 11.5 Sv (Fig. 2a, b, red solid lines), which is roughly consistent with the estimates from the IPCC models under the Scenario A1B (Schmittner et al. 2005). Then the AMOC recovers slightly and slowly to reach a final value of 12.7 Sv in the rest of the simulation. The ultimate decrease is 2.7 Sv (18 %). For the LGM, in LGM-2CO2, the AMOC first decreases by 8 % at the year 90 from 12.7 to 11.7 Sv (Fig. 2a, b, blue solid lines). After that, the AMOC strengthens in two stages: a rapid increase stage from 11.7 to 15.8 Sv in the next 300 years, and a subsequent slow increase to 17.4 Sv till year 1,500. It seems that the responses of the AMOC in both MOD-2CO2 and LGM-2CO2 have reached quasi-equilibrium by the end of the simulation, with the changing rates in the last 500 years of 0.07 and 0.09 Sv century^{-1}, respectively. The distinct structures of the AMOC responses can be seen in the meridional overturning streamfunction (Fig. 3c–f). In MOD-2CO2, the AMOC weakens significant in the first 100 years and recovers slightly in the rest of the simulation (Fig. 3c, e). In LGM-2CO2, the AMOC weakens slightly in the first 90 years, but the quasi-equilibrium state shows a much stronger AMOC (Fig. 3d, f). It should be pointed out that, although a coarse resolution model is employed in this study, the response of the AMOC in MOD-2CO2 qualitatively agrees with results from CCSM3 with higher resolutions (Bryan et al. 2006), the newer CCSM4 (Meehl et al. 2012) and Community Earth System Model version 1 (CESM1) (Meehl et al. 2013), and many other Coupled Model Intercomparison Project Phase 5 (CMIP5) models (Collins et al. 2013). Nevertheless, the long-term (millennial-timescale) response of the AMOC and the responsible physical mechanism in the modern climate still differ greatly in different climate models and studies (Rahmstorf

and Ganopolski 1999; Voss and Mikolajewicz 2001; Stouffer and Manabe 2003; Wood et al. 2003; Yang and Zhu 2011; Weaver et al. 2012).

It is important to emphasize that the response timescales of the AMOC also differ substantially between the modern and glacial climates. The response of the AMOC in MOD-2CO2 can be divided conveniently into two stages: an initial rapid weakening (the first 100 years, at the rate -4.0 Sv century^{-1}) and a subsequent slow strengthening stage (100–1,500 years, at the rate of 0.1 Sv century^{-1}). In contrast, the response of AMOC in LGM-2CO2 should be divided into three stages: an initial rapid weakening stage (the first 90 years), a following rapid increasing stage (91–400 years) and a final slow strengthening stage (401–1,500 years) with changing rates of -1.1, 1.3 and 0.1 Sv century^{-1}, respectively. Therefore, the responses of the AMOC show a common initial fast weakening and a final slow strengthening stage in both MOD-2CO2 and LGM-2CO2. But, the AMOC has a strong intensification stage between the initial and final stages in LGM-2CO2. In these two doubling CO_2 experiments, the initial radiative forcing is the same and the only difference is the background climate states, i.e., one is glacial and the other is modern climate. Therefore, the different responses of the AMOC must be caused by the different climate states.

The final slow strengthening of the AMOC in LGM-2CO2 is consistent with the overall evolution in the transient TraCE-GHG simulation (Fig. 1) and the aforementioned studies (Knorr and Lohmann 2007; Banderas et al. 2012). However, LGM-2CO2 does reveal the existence of an initial weakening stage at the LGM with a period of $\sim$100 years, which is not captured by the first part of TraCE-GHG due to the gradual changing of the forcing. In the last 150 years of TraCE-GHG, the rapid increase of atmospheric CO_2 leads to a decrease of the AMOC, consistent with the initial weakening in LGM-2CO2, as well as in MOD-2CO2.

In short, the experiments in CCSM3 show that the AMOC responds significantly differently to the increase of CO_2 under the modern and LGM states, and at different timescales. In the following, we will examine the mechanisms that cause these differences by firstly analysing changes in the surface density flux in Sect. 4 and then diagnosing the density changes in Sect. 5.

4 Surface density fluxes and the AMOC evolution

4.1 Density flux and implied water mass formation in the control experiments

We first attempt to understand the evolution of the AMOC in light of the surface density flux and the associated water mass formation (Schmitt et al. 1989; Speer and Tziperman 1992) in the Atlantic Ocean. The density flux measures the loss/gain of water mass of the ocean surface layer due to the heat and freshwater/salt exchanges with other components, e.g., the atmosphere, land and sea ice. The density flux is calculated from the linearized equation of state (EoS) of seawater as,

$$F_\rho = -\alpha \cdot \frac{Q}{C_p} + \rho(0,T) \cdot \beta \cdot \frac{(E-P-R-I)\cdot S}{1-S} \qquad (1)$$

In the above equation, Cp, T and S are the specific heat capacity, surface temperature and salinity of seawater, respectively. $\alpha = -\frac{1}{\rho}\left(\frac{\partial \rho}{\partial T}\right)_{p,S}$ and $\beta = \frac{1}{\rho}\left(\frac{\partial \rho}{\partial S}\right)_{p,T}$ are the thermal expansion and haline contraction coefficients. $\rho(0,T)$ is the density of freshwater with salinity of 0 and temperature of T. Q represents the surface heat flux, and E, P, R and I denote the freshwater fluxes due to evaporation, precipitation, river run-off and sea-ice melting and brine rejection, respectively. The first part in the right hand side of Eq. (1) is the thermal density flux, and the second part is the haline density flux. For simplicity, we employ a linear EoS of seawater in this study, but one should keep in mind that nonlinear processes could be another source of dense water formation (Klocker and McDougall 2010). Considering that the buoyancy source/sink due to nonlinearities of EoS is insignificant at the surface ocean (Hieronymus and Nycander 2012), our major results should not vary when a nonlinear EoS of seawater is adopted. The density flux-implied water mass formation rate as a function of the surface density is defined as,

$$M_B(\rho) = \frac{1}{\Delta\rho}\sum A \cdot F_\rho \cdot \delta[(\rho+\Delta\rho)-\rho] \qquad (2)$$

where, ρ is the surface density of seawater, and A is the surface area of the density interval between ρ and $\rho+\Delta\rho$ (the interval is 0.1 kg m^{-3} in this study). The delta-function is used to collect the density flux within the density intervals.

The surface density flux in the Atlantic Ocean differs significantly between the control experiments for the modern and LGM climates (Fig. 4), largely because of the different sea-ice extent. In MOD, the density flux (Fig. 4a, shading) in the North Atlantic is dominated by the thermal component (Fig. 4b, shading), while the haline density flux (Fig. 4c, shading) is significant only along the annual sea-ice margin. There are two convection centres in the North Atlantic indicated by the March mixed layer depth (black contours): a major center to the south of Greenland with a maximum depth larger than 1,200 m and a minor center in the GIN Seas with a mixed layer depth of over 400 m. However, at the LGM, there is a strong negative density flux centre in the mid-latitude around 40°N (Fig. 4d)

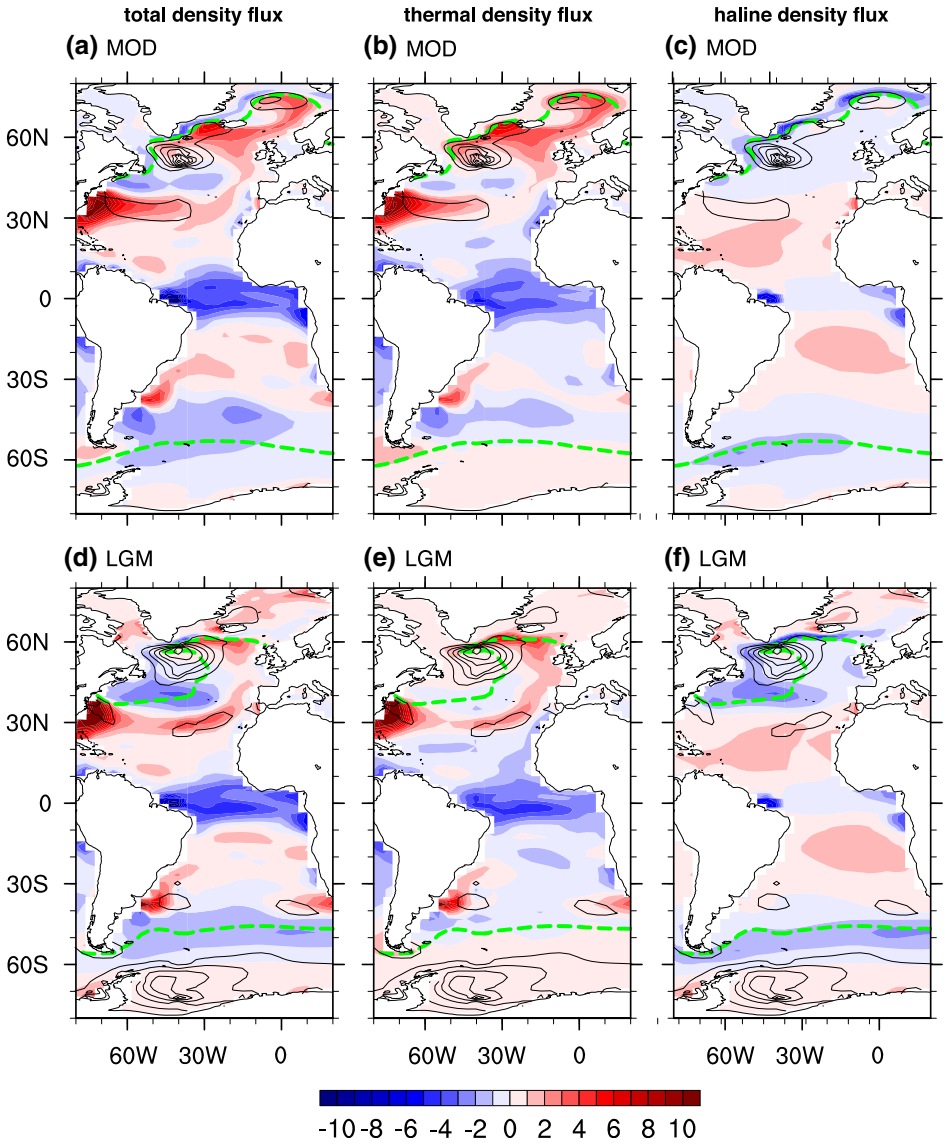

Fig. 4 *Shading* represents the Atlantic surface density flux in the control experiments, **a** the total density flux, **b** the thermal density flux and **c** the haline density flux in the modern climate (units: 10^{-6} kg m^{-2} s^{-1}). The *black contours* are the March and September mixed layer depth for the Northern and Southern Hemisphere, respectively, and the contour interval is 200 m. The *green contours* depict the annual mean sea-ice margin (defined as 15 % sea-ice coverage). **d**, **e** and **f** are the same, but for the LGM. Note that data of the last 100 years from each control simulation is used to generate its climatology, and the results do not depend on the choice of time period, because the trend in the surface state variables is very small

produced mainly by the melting of sea ice (see also Figs. 11b, 12b) and the resulting haline density flux (Fig. 4f). The convection centre in the GIN Seas disappears, due to the extensive sea ice that shields the heat loss to the atmosphere (Fig. 4d, green contour). Another significant difference between the LGM and modern climates occurs in the Southern Ocean (Fig. 4a, d). At the LGM, the deep convection and water mass formation is much greater in the Weddell Sea, corresponding to the stronger AABW, which is caused by the stronger brine rejection during glacial climate (Shin et al. 2003a).

The comparison of density flux-implied AABW formation in the South Atlantic between the modern climate and the LGM is similar with Shin et al. (2003a); however substantial difference does exist in the North Atlantic (Fig. 5). The AABW formed in the Weddell Sea is quite small in MOD (Fig. 5b, red solid line), and it is much stronger and forms between the surface density of 1,029.4 and 1,029.7 kg m^{-3} at the LGM (blue solid line) due to the saltier water mass during glacial period. The peak value of the Glacial North Atlantic Intermediate Water (GNAIW) at the LGM, formed between the potential density of 1,028.2 and 1,028.9 kg m^{-3} (Fig. 5a, blue solid line), is approximately 40 % weaker than the NADW in MOD, formed between 1,026.6 and 1,027.5 kg m^{-3} (red solid line). It suggests that processes in the North Atlantic are potentially involved in determining the glacial water mass formation and the strength of the AMOC, and possibly could influence the response of glacial AMOC to the increase of atmospheric CO_2. In contrast, Shin et al. (2003a) reported that, in their simulations, the water mass formation in the North Atlantic does not change much between the LGM and modern climates; therefore, they argue that the weaker glacial AMOC is produced by the southern control processes.

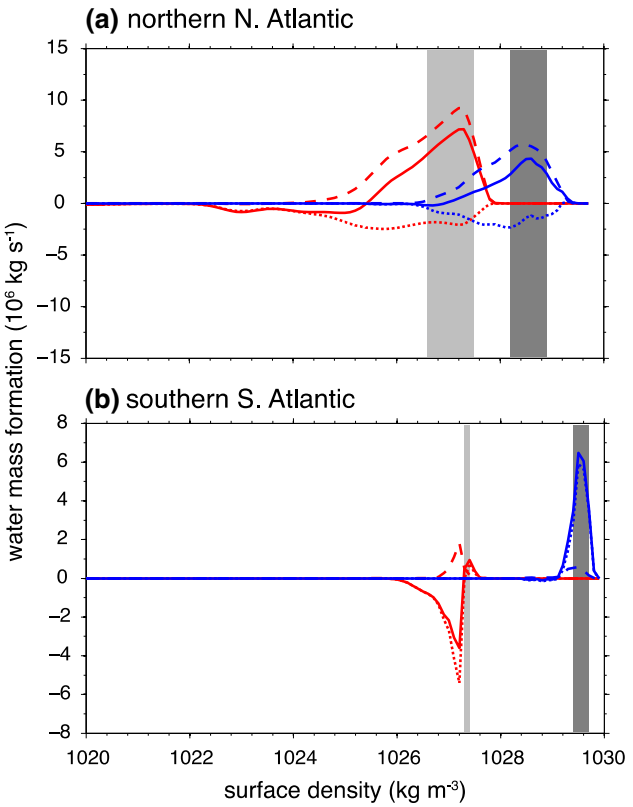

Fig. 5 The water mass formation rate in the northern North Atlantic Ocean (**a**) and the southern South Atlantic Ocean (**b**) diagnosed from the surface density flux in the control experiments for the modern climate (*red*) and LGM (*blue*). The *solid*, *dashed* and *dotted lines* are for the total, thermal and haline density flux, respectively. The *light gray bins* indicate the density intervals for the North Atlantic deep water in the north and the Antarctic Bottom Water in the south in modern climate. The *dark gray bins* are the same, but for the LGM. Note that data of the last 100 years from each control simulation is used, and the results do not depend on the choice of time period

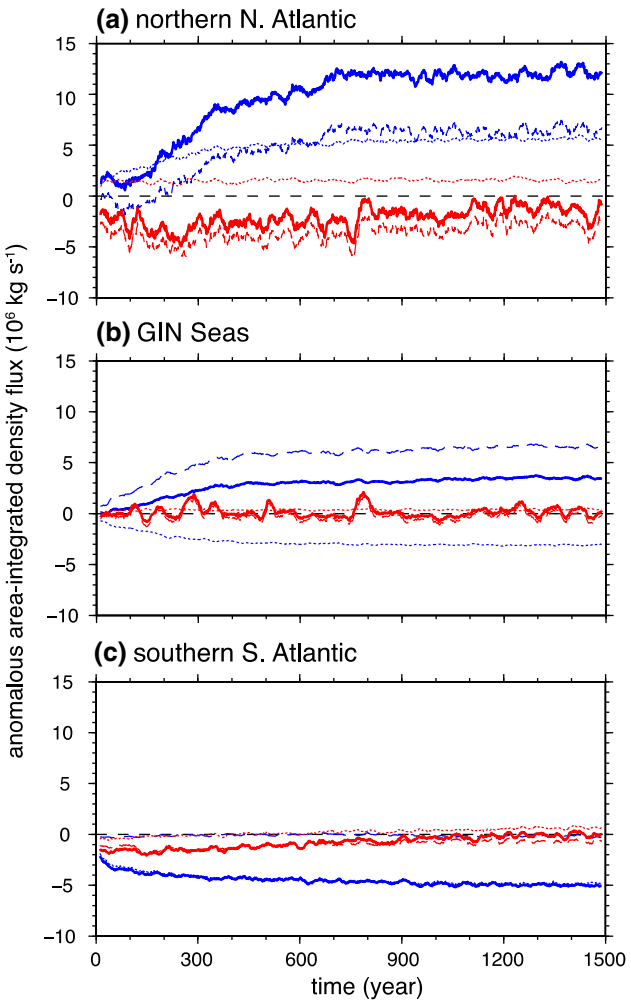

Fig. 6 The anomalous area-integrated density flux in the northern North Atlantic Ocean including the Labrador Sea (**a**), the GIN Seas (**b**) and the southern South Atlantic Ocean (**c**) in the doubling CO_2 experiments for the modern climate (*red*) and LGM (*blue*). The *solid*, *dashed* and *dotted lines* are for the total, thermal and haline density flux, respectively

4.2 Changes of density flux in MOD-2CO2 and LGM-2CO2

In order to investigate the mechanisms for the distinct responses of AMOC in doubling CO_2 experiments, we calculate the area-integrated density flux in the northern North Atlantic Ocean (30°N northward and including the Labrador Sea), the GIN Seas and the southern South Atlantic Ocean (50°S southward). In MOD-2CO2, the most significant changes happen in the northern North Atlantic Ocean (Fig. 6a, red lines), with the GIN Seas and the southern South Atlantic showing little response (Fig. 6b, c, red lines). In response to the CO_2 increase, the thermal density flux decreases in the North Atlantic subpolar region due to the green house effect (Fig. 7b), but the haline density flux increases along the sea-ice margin because of the decreased meltwater associated with sea-ice retreat (Fig. 7c; Bryan et al. 2006). The reduction of thermal density flux (Fig. 6a, red dashed line) is almost twice as much as the increase of haline density flux (red dotted line) in the initial 200 years, such that the total density flux (red solid line) is reduced initially. This dominant role of the surface heat flux in weakening the North Atlantic water mass formation and the AMOC agrees with the IPCC models (Gregory et al. 2005; Weaver et al. 2007). After 200–300 model years, the magnitude of the (negative) thermal density flux decreases gradually, weakening the total (negative) density flux slowly. The evolution of the density flux in the northern North Atlantic Ocean coincides very well with behaviors of the AMOC. Previous study (Bryan et al. 2006) suggests that the slow recovery of the AMOC could be caused by the reduced northward heat and freshwater transports by the AMOC.

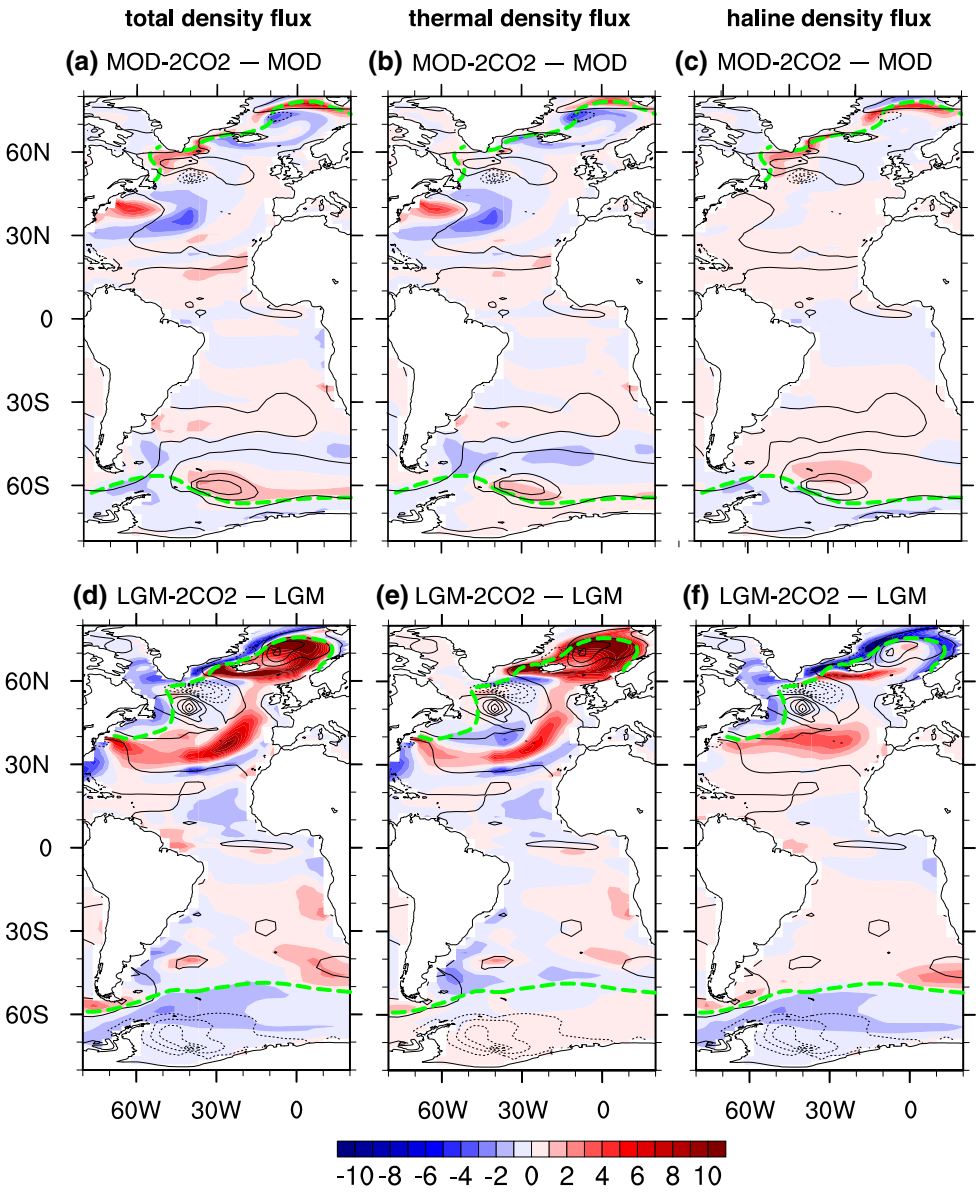

Fig. 7 *Shading* represents the anomalous Atlantic surface density flux in the doubling experiments, **a** the total density flux, **b** the thermal density flux and **c** the haline density flux in modern climate (units: 10^{-6} kg m^{-2} s^{-1}). The *black contours* are the final changes in March and September mixed layer depth for the Northern and Southern Hemisphere, respectively, and the contour interval is 200 m. The *blue contours* depict the annual mean sea-ice margin (defined as 15 % sea-ice coverage) averaged in the final 100 years in doubling CO_2 experiments. **d**, **e** and **f** are the same, but for the LGM

In the northern North Atlantic, both the increased haline density flux (Fig. 6a, blue dotted line) and thermal density flux (blue dashed line) could possibly contribute to the strengthening of the AMOC in LGM-2CO2 starting around year 90. The much larger increase of the haline density flux in the glacial climate (blue dotted line vs red dotted line) is caused by a greater sea-ice retreat and meltwater reduction (Fig. 7f). The thermal density flux in the northern North Atlantic Ocean (blue dashed line) starts to increase after about 100 years and switches to positive around year 200 and continues to increase, reaching quasi-equilibrium approximately at year 700. At first sight, it seems counterintuitive that the ocean is losing heat in a warming climate due to the increased CO_2 at the LGM. This can be attributed to the insulating effect of sea ice (Lohmann and Gerdes 1998; Jayne and Marotzke 1999; Banderas et al. 2012; Oka et al. 2012), as discussed below. At the LGM, the annual mean sea-ice covers the northwestern North Atlantic Ocean, and the entire Labrador Sea and the GIN Seas, constituting 51 % of the North Atlantic subpolar region (Table 1; Fig. 4d), which agrees well with the reconstructions (Sarnthein et al. 2003). Therefore, the doubling of CO_2 leads to a dramatic sea-ice retreat (Fig. 7), which exposes much seawater to lose heat directly to the atmosphere. When the sea-ice retreat is sufficiently large, the increased density flux by the heat loss could overwhelm the decreased from the warming of doubling CO_2. This is not the case in the modern climate, because of a much smaller sea-ice cover (22 %) with the northwestern North Atlantic Ocean and a large portion of the GIN Seas already exposed to atmosphere (Table 1; Fig. 4a). In the first 200 years, the decrease of thermal density flux in LGM-

2CO2 (blue dashed line) is much smaller than that in MOD-2CO2 (red dashed line), likely caused by the stronger insulating effect from the sea ice (Fig. 4) and the much smaller thermal expansion coefficients at the LGM. One may note that the area-integrated net change of density flux increases (positive, blue solid line) in the first several decades when the AMOC is weakening in LGM-2CO2. This is because the density flux is integrated over a large area of the North Atlantic to accommodate the potential impact of remote density fluxes at longer timescales. If integrated only over the deep-water formation regions (density intervals indicated in Fig. 5a), the surface density flux indeed decreases as the AMOC does (not shown).

In the GIN Seas, the thermal density flux (Fig. 6b, blue dashed line) could also potentially contribute to the strengthening of AMOC in LGM-2CO2. Similarly, it could be owing to the retreat of sea ice and the subsequent intensification of heat loss to the atmosphere (Fig. 7e). The integrated haline density flux in LGM-2CO2 (blue dotted line and Fig. 7f) decreases, because of the increased meltwater flux and the decreased brine rejection from the sea ice in a warmer climate. In MOD, there are much less sea ice and, therefore, the retreat of sea ice and changes in thermal and haline density flux (red lines) are insignificant.

In the Southern Ocean, the decrease of density flux (Fig. 6c, blue solid line) and the implied weakening of the AABW could be another factor that potentially causes the intensification of AMOC in LGM-2CO2. This reduced density flux in the south is primarily contributed by the reduction of brine rejection (blue dotted line and Fig. 7f) in response to doubling CO_2. In MOD-2CO2, originally the deep-water formation is much weaker than that at the LGM. When we double the atmospheric CO_2, the weakening effect from haline density flux (red dotted lines) is unnoticeable. However, as discussed earlier (Stouffer 2004; Liu 2006), the impact of density flux in the Southern Ocean on the decreased AABW, and potentially the AMOC should only be fully active at millennial timescales. Therefore, the response of density flux in the Southern Ocean here is unlikely to trigger the rapid intensification of the AMOC starting at year 90, but could contribute significantly at longer timescales.

To summarize, the above discussion on the surface density fluxes suggests, from an oceanic perspective, that the increased (decreased) heat flux (thermal density flux) in the northern North Atlantic Ocean (Fig. 6a, dashed lines) could be the only driver for the initial weakening of the AMOC in both climates, while the rapid intensification in LGM-2CO2 could be potentially contributed by two processes in the north: (1) the positive haline density flux due to the reduced meltwater in the northern North Atlantic (Fig. 6a, blue dotted line and Fig. 7f), (2) the positive thermal density flux in the northern North Atlantic (Fig. 6a, blue dashed line and Fig. 7e) and the GIN Seas (Fig. 6b, blue dashed line and Fig. 7e). Both processes are associated with a greater retreat of sea-ice coverage at the LGM, but their relative contributions are still unknown. Although it is useful, we should keep in mind that the surface fluxes and water mass formation could be functions of the ocean circulation itself, i.e., the ocean circulation can regulate the surface exchange through its heat and freshwater transport (Saenko et al. 2004). For example, the reduction of meltwater in the northern North Atlantic could drive the intensified AMOC and the increased northward heat transport, which could melt the sea ice in the north and, therefore, enhance the thermal density flux. So, the enhanced heat loss could be a result of the intensified AMOC, instead of a driving force. Next, through diagnosing changes in the subsurface density, temperature and salinity, we will show that it is indeed this case.

5 Subsurface densities and the AMOC evolution

To understand the relative importance of surface heat and freshwater fluxes in determining the intensification of the AMOC in LGM-2CO2, we now further proceed to study changes of zonal mean potential density in the Atlantic Ocean, assuming that it is the north–south (N–S) density contrast in the upper ocean that drives changes in the AMOC (Bryan et al. 2007 and references therein). Based on the evolution of the AMOC in MOD-2CO2 and, in particularly, in LGM-2CO2, we will examine changes in zonal mean density and their relationship with the AMOC in three stages: the initial (1–90 years), the intermediate (91–400 years) and the final stage (401–1,500 years). Moreover, we will evaluate the relative contributions by estimating the temperature- and salinity-induced density changes from the linearized EoS of seawater (Figs. 8, 9, 10). We further quantify the N–S density difference within a northern (35°N–65°N) and a southern box (0°N–30°N) in the Atlantic Ocean. Both of them span from surface to 1,000 m depth, where the AMOC reaches maximum. Our results suggest a very good agreement between the response in the AMOC and changes in the N–S density contrast for both climates (Table 2), with a correlation coefficient for LGM-2CO2 as large as 0.9. The density changes that cannot be explained by the linearized EoS are denoted as residual, which generally is much smaller than the linear contributions (Table 2) and, therefore, should not alter our findings.

5.1 The initial stage (1–90 years)

In the initial stage, the decrease of the Atlantic upper ocean density in LGM-2CO2 is analogous to that in MOD-2CO2

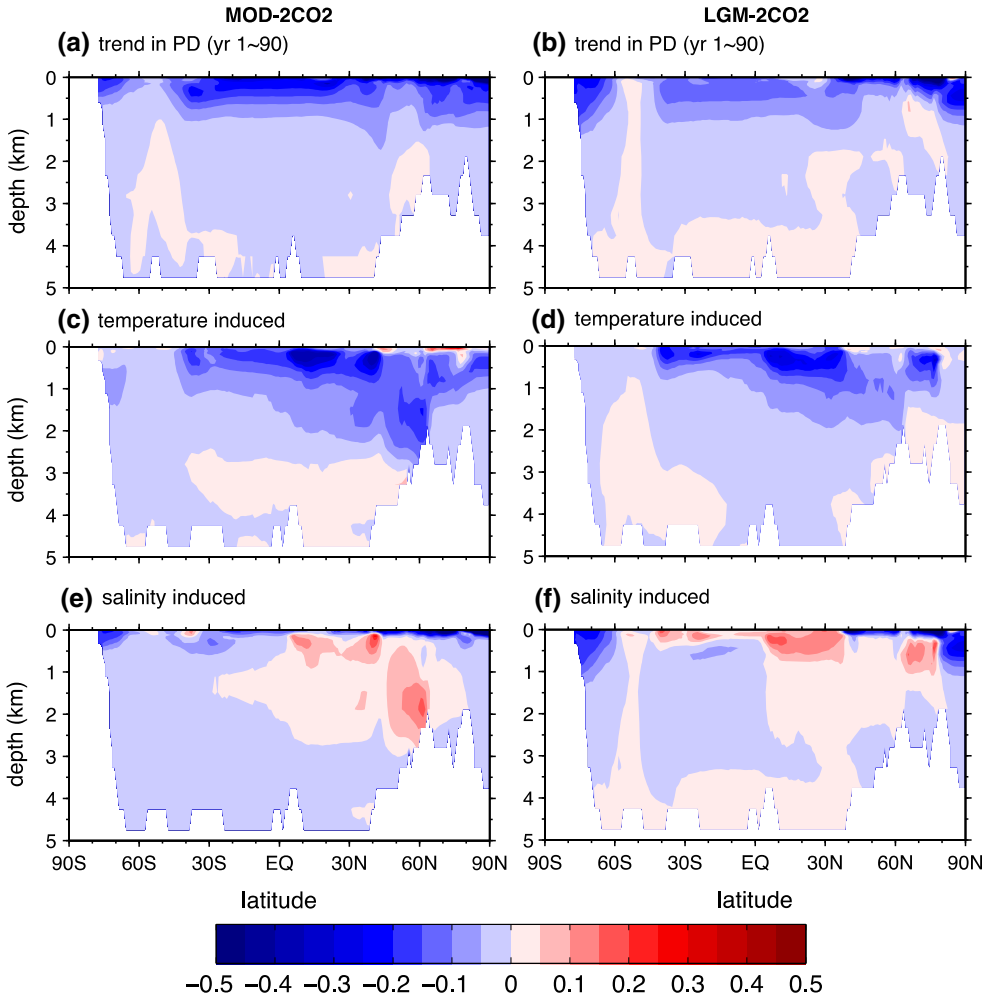

Fig. 8 Linear changes in the first 90 model years in the Atlantic zonal mean potential density (**a**), temperature-induced (**c**) and salinity-induced (**e**) density changes in the doubling CO_2 experiments for the modern climate. The contour interval is 0.05 kg m^{-3}. **b**, **d** and **f** are the same, but for the LGM

(Fig. 8a, b). The decrease of density diminishes primarily with depth and is greater in high latitudes owing to the stronger ventilation there. Calculation demonstrates that the density in the northern box decreases more than that in the southern box by −0.01 to −0.02 kg m^{-3}, favouring a weaker N–S density contrast (Table 2), consistent with the weakening of the AMOC during this period. For both experiments, the decrease of density can be attributed mainly to the warming of the upper ocean (negative temperature-induced density change, Fig. 8c, d) and partly to the freshening of the surface ocean in high latitudes (Fig. 8e, f; Table 2). At this stage, the radiative forcing from doubling CO_2 is responsible for the consistent warming of the upper ocean (see also Fig. 11a). Additionally, the reduced AMOC and the subsequent reduction of heat transport could act to warm the southern box more and cool the northern box (Fig. 11a and discussion in Appendix 1). The role of subsurface salinity changes is to partly counteract the temperature-induced weakening of the N–S density contrast, and it is similar between the LGM and modern climate (Table 2). The fact that the decrease of N–S density contrast is dominated by the temperature changes in the northern box supports the predominant role of heat flux during this period (Sect. 4.2), especially considering that the reduced convergence of heat transport acts to increase the density (a negative feedback). It is worth noting that the decrease of salinity and density in the south is much stronger in LGM-2CO2, consistent with the much greater reduction of haline density flux in the south (Figs. 6c, 7f), but its impact on the AMOC is negligible at this initial short timescale.

5.2 The intermediate stage (91–400 years)

Changes in the Atlantic zonal mean density diverge greatly in the next 300 years between MOD-2CO2 and LGM-2CO2 (Fig. 9). In MOD-2CO2, the density (Fig. 9a) keeps decreasing, but at a lower rate, and the signal penetrates deeper (~2,000 m), which is still dominated by the temperature changes (Fig. 9c, e; Table 2). In contrast, the density in LGM-2CO2 starts to increase substantially in the north (Fig. 9b, by 0.09 kg m^{-3} in Table 2), primarily due

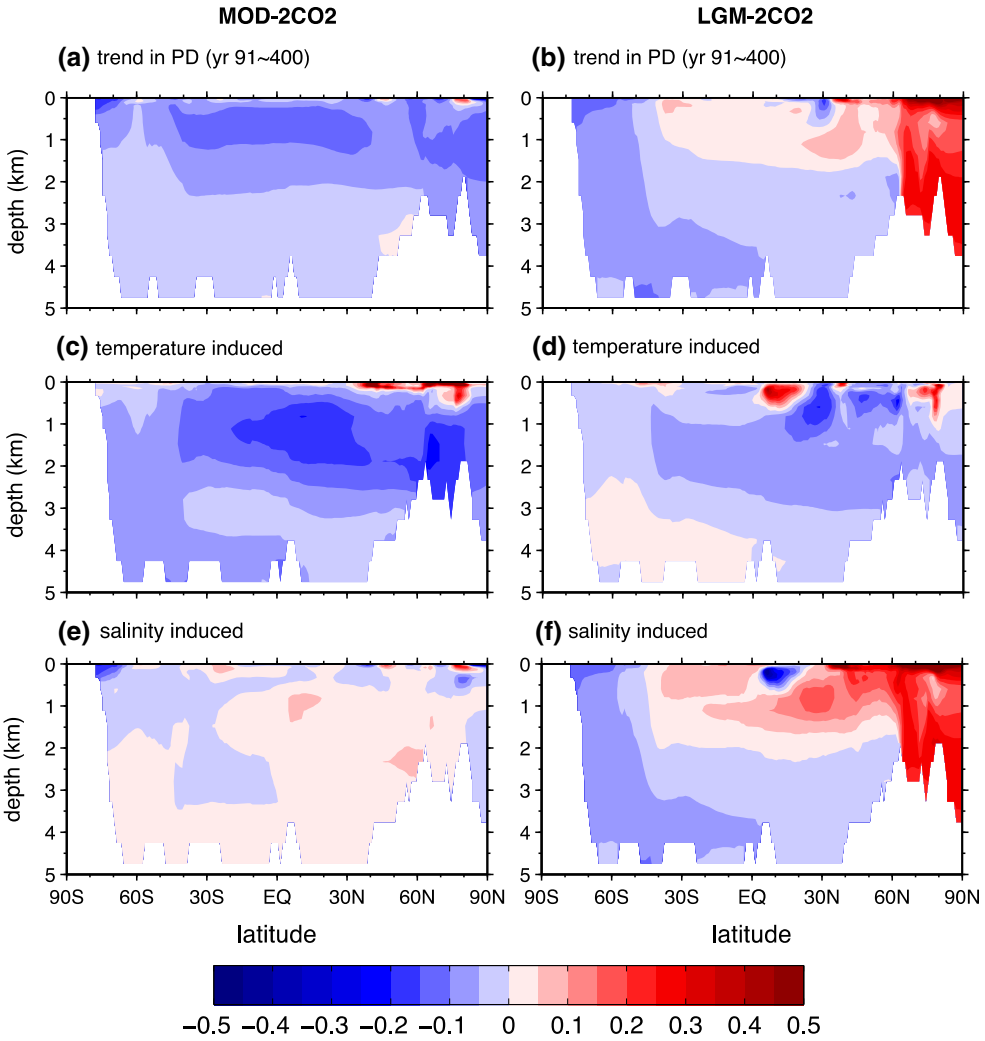

Fig. 9 Linear changes between the 91 and 400 model year in the Atlantic zonal mean potential density (**a**), temperature-induced (**c**) and salinity-induced (**e**) density changes in the doubling CO_2 experiments for the modern climate. The contour interval is 0.05 kg m^{-3}. **b**, **d** and **f** are the same, but for the LGM

to the contribution from increased salinity (Fig. 9f, 0.2 kg m^{-3} in Table 2). Meanwhile, the temperature-induced density (temperature) decreases (increases) more in the northern box, which is likely to be related to the enhanced AMOC and northward heat transport (Fig. 11a). Clearly, changes in salinity act to increase the N–S density contrast and the AMOC in LGM-2CO2, while changes in temperature counteract this effect (Table 2). The negative contribution of temperature changes implies that changes in surface heat flux do not drive the intensification of the AMOC; instead, they are results of the increased AMOC and northward heat transport during this stage. The decrease of salinity and density in the Southern Ocean is still much stronger in LGM-2CO2 and penetrates deeper during this period. The next questions would be what causes the increase of salinity in the north and what is the role of surface freshwater flux and transport by ocean circulations? We will discuss these questions in Sect. 5.4 after we describe the evolution of the Atlantic zonal mean density during the final stage.

5.3 The final stage (401–1,500 years)

The increase of N–S density contrast in LGM-2CO2 keeps developing during the final stage (Fig. 10b; Table 2), mostly because of salinity changes as well (Fig. 10f), with changes in temperature inconsequential (Fig. 10d). The most striking feature different from the intermediate stage is that the penetration of the negative density anomaly extends from the Southern Ocean into the bottom ocean and further north in the North Atlantic, similar to the simulation in CCSM1 (Shin et al. 2003a, b; Liu et al. 2005). This distinct basin-scale N–S asymmetric response in density, decreasing in the southern and bottom ocean and increasing in the upper and northern ocean, could further strengthen the AMOC gradually during this period. In comparison, the density anomaly also reaches the bottom ocean in MOD-2CO2 (Fig. 10a), but primarily due to the warming (Fig. 10c), rather than the salinity changes (Fig. 10e); furthermore, there is no significant N–S asymmetry in zonal mean density response (Table 2).

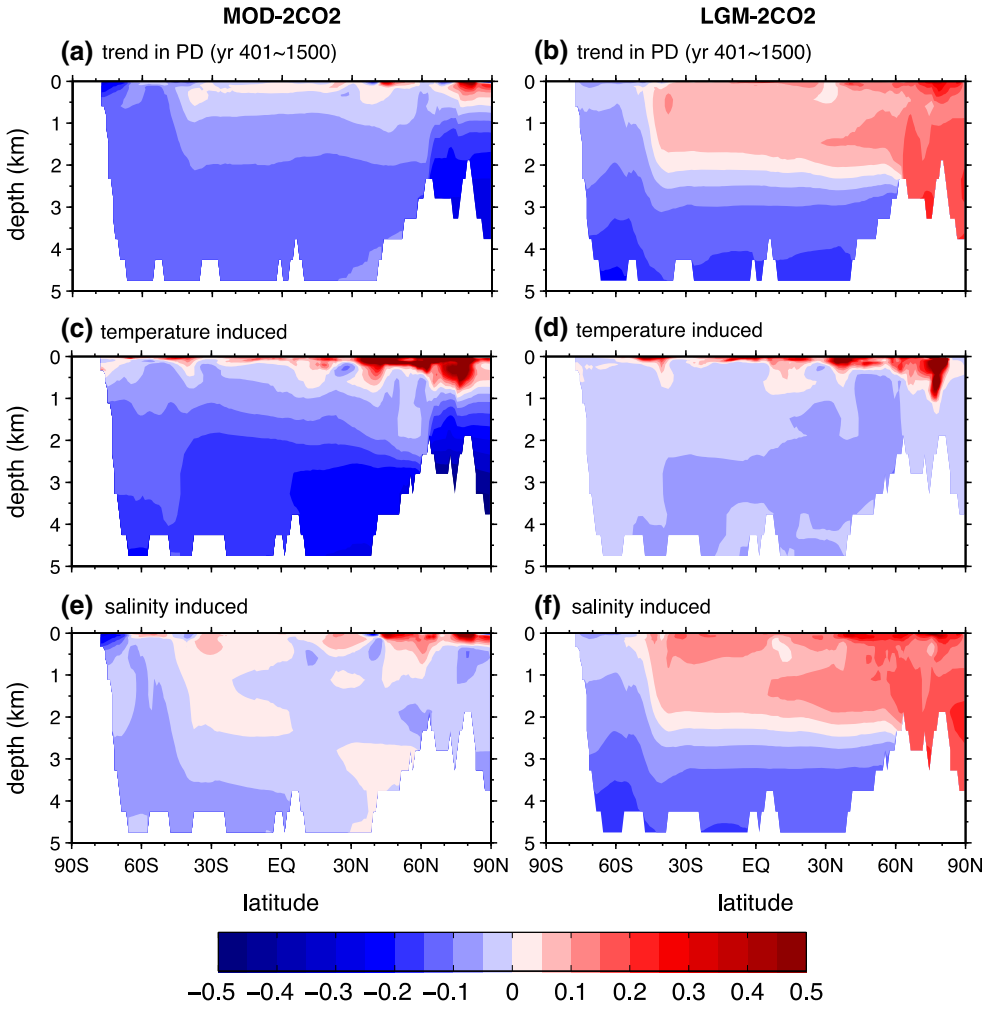

Fig. 10 Linear changes between the 401 and 1,500 model year in the Atlantic zonal mean potential density (**a**), temperature-induced (**c**) and salinity-induced (**e**) density changes in the doubling CO_2 experiments for the modern climate. The contour interval is 0.05 kg m^{-3}. **b**, **d** and **f** are the same, but for the LGM

Table 2 Changes in the AMOC (units: Sv), north–south density contrast ($\Delta\rho$) and density in the northern (35°N–65°N, ρ_N) and southern box (0°N–30°N, ρ_S), and temperature- and salinity-induced density ($\rho_{N,S}(T)$ and $\rho_{N,S}(S)$, units: 10^{-1} kg m^{-3}) in the upper (1,000 m) North Atlantic Ocean for the doubling CO_2 experiments at three stages

	MOD-2CO2				LGM-2CO2			
	AMOC	$\Delta\rho$, ρ_N, ρ_S	$\rho_N(T)$, $\rho_N(S)$, residual	$\rho_S(T)$, $\rho_S(S)$, residual	AMOC	$\Delta\rho$, ρ_N, ρ_S	$\rho_N(T)$, $\rho_N(S)$, residual	$\rho_S(T)$, $\rho_S(S)$, residual
Initial (1–90 years)	−2.7	**−0.14**	**−1.54**	−1.8	−1.0	**−0.20**	**−1.07**	−1.77
		−1.53	*−0.10*	0.36		**−1.01**	−0.10	0.84
		−1.39	0.11	0.05		−0.81	0.16	0.12
Intermediate (91–400 years)	0.5	*0.02*	−0.98	−1.32	4.0	**0.75**	−1.28	−0.13
		−1.01	−0.10	0.19		**0.90**	**2.02**	0.23
		−1.03	−0.07	0.10		0.15	0.16	0.05
Final (401–1,500 years)	0.8	0.17	−0.33	−0.24	1.6	**0.23**	−0.57	−0.09
		−0.06	0.24	0		**1.00**	**1.49**	0.85
		−0.23	0.03	0.01		0.77	0.08	0.01

The residual term represents the density change due to the nonlinearities of the equation of state of seawater. Numbers in italic are not significant at 95 % level. Important processes that cause changes in the AMOC are highlighted in bold

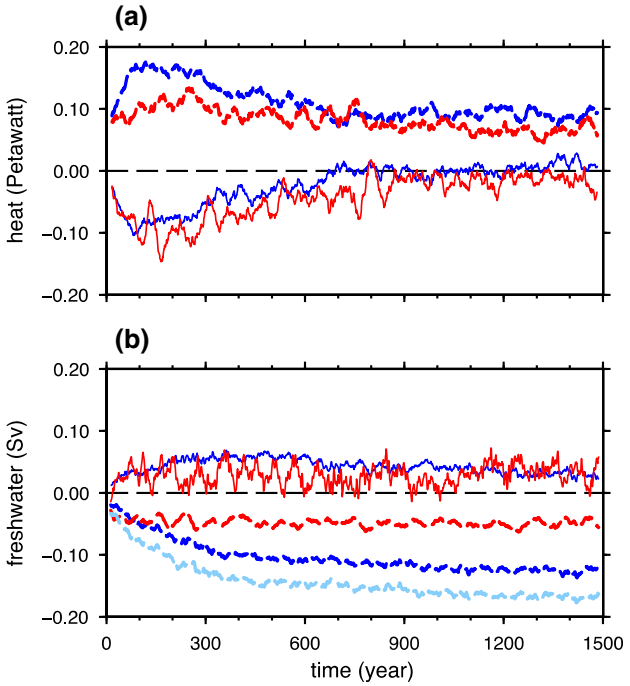

Fig. 11 **a** Convergence of anomalous northward heat transport (*solid*) in the northern box (35°N–65°N, 1,000 m upward) in the Atlantic Ocean and changes in surface heat flux (*dashed*) in the doubling CO_2 experiments for the modern climate (*red*) and LGM (*blue*). **b** The same as **a**, but for the freshwater flux and transport. The *light blue line* represents the anomalous surface freshwater flux from the meltwater for the LGM

5.4 Surface flux versus transport

Our findings reveal that the increase in salinity over the North Atlantic deep-water formation region in LGM-2CO2 is contributed mainly by the decrease in surface freshwater flux, rather than the changes in freshwater transport of ocean circulations. To directly demonstrate this, we calculate the surface freshwater flux and the convergence of freshwater transport for the northern box in the North Atlantic Ocean, which is shown in Fig. 11b (a quantitative analysis including the southern box can be found in the Appendix 1). In LGM-2CO2, the decrease in surface freshwater flux accelerates from −0.03 Sv at year 90 to −0.10 Sv at year 400, and reaches −0.12 Sv till the end of the simulation (blue dashed line), which is predominantly from the reduction of meltwater flux (light blue dashed line). Meanwhile, there is a net freshwater convergence of ∼0.05 Sv at year 400 by transport (blue solid line). Therefore, the freshwater transport contributes a negative feedback to freshen the subpolar North Atlantic and slowdown the AMOC, while the surface freshwater flux acts to increase the salinity and the AMOC. More importantly, a positive sea ice–ocean coupled feedback could amplify the strengthening of the AMOC: the increased AMOC after the initial weakening could transport more heat northward (Fig. 11a) and cause more sea-ice retreat and less meltwater flux, which, in turn, could further intensify the AMOC (Yang and Neelin 1993). The same processes, however, are insignificant for the modern climate, because the reduction of meltwater flux in the northern box is only 30 % of that at the LGM (Fig. 11b, red dashed line).

In addition to the coupled sea ice–ocean positive feedback associated with meltwater flux, other feedbacks with various strength are also involved (Swingedouw et al. 2007). Although the convergence of freshwater transport in LGM-2CO2 acts as a negative feedback to freshen the northern North Atlantic and reduce the AMOC (Fig. 11b), it is a residual of a strong positive feedback associated with the freshwater transport (salt advection) by the AMOC and a strong negative feedback associated with the azonal transport (see Table 4 and discussion in Appendix 1). For both the MOD-2CO2 and LGM-2CO2, changes in the convergence of heat transport are negative during the initial stage, indicating a negative feedback between the strength of the AMOC and heat transport. It is interesting to note that during the intermediate strengthening stage in LGM-2CO2, the surface heat flux decreases significantly, which suggests a positive feedback between the AMOC and the surface heat flux associated to the sea-ice insulating effect (see Table 3 and discussion in Appendix 1). Nevertheless, the coupled sea ice–ocean feedback associated with meltwater flux is the most important mechanism for the rapid strengthening of the AMOC during the intermediate stage, as the density changes in the northern North Atlantic is primarily generated by the salinity changes and the removal of freshwater is dominated by the reduction of surface meltwater flux.

6 Summary and discussion

Our sensitivity experiments have demonstrated that the behavior of the AMOC to CO_2 increase and global warming may vary greatly depending on the timescale of the response and the background climate state, i.e., the modern climate and the LGM. In the modern climate, after the doubling of atmospheric CO_2, the AMOC first decreases (by 25 %, 4 Sv) in the first 100 years and then recovers slowly (by 6 %, 1 Sv) in the remaining of the 1,500-year simulation. At the LGM, the AMOC weakens in the initial 90 years (by 8 %, 1 Sv), but then it reverses to intensification first rapidly (by 30 %, 4 Sv) in the next 300 years, and then slowly (by 13 %, 1.6 Sv) during the remainder of the integration. It is suggested that the responses of the AMOC in both climates have a similar initial rapid weakening period of ∼100 years and a similar

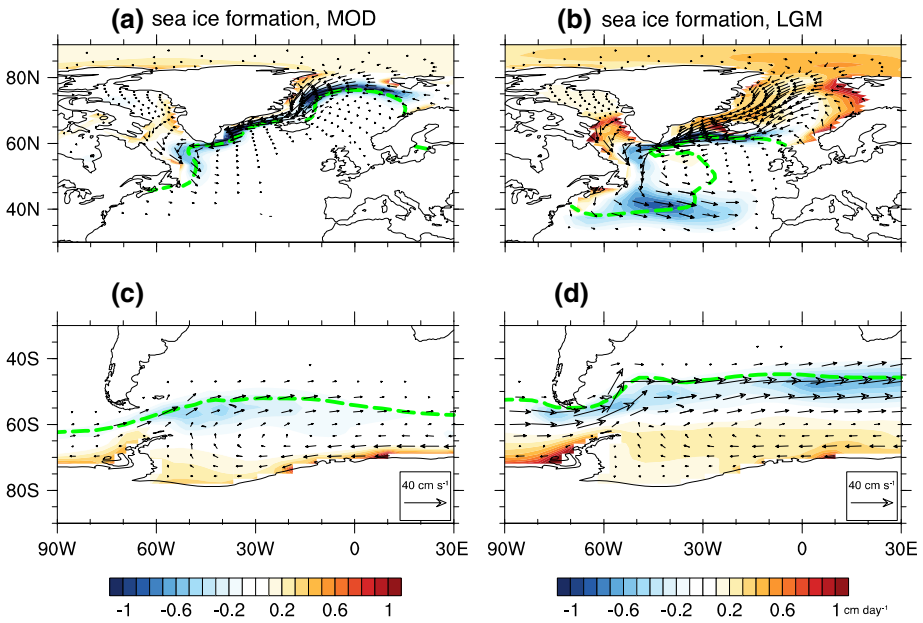

Fig. 12 **a** and **c** show the annual mean sea-ice formation rate (*shading*, units: cm day^{-1}), the sea-ice velocity (*vectors*, units: cm s^{-1}) and the sea-ice margin (*green contours*, defined as the 15 % sea ice-fraction) in the Atlantic Ocean in the control simulation for the modern climate, **b** and **d** are the same, but for the LGM

final slow strengthening period over 1,000 years long. However, LGM has an additional intermediate stage with rapid intensification (~300 years). The rapid intensification starting from the 90th year is triggered and sustained by a coupled sea ice–ocean feedback associated with surface meltwater flux: the reduction of meltwater in the northern North Atlantic due to sea-ice retreat could increase the AMOC and northward heat transport, which, in turn, could cause more sea-ice retreat and reduction of meltwater. These processes, however, are insignificant under modern conditions. After the initial weakening period at the LGM, the changes in heat flux in the northern North Atlantic is only a response to the increased AMOC, instead of a driving force.

At centennial-millennial timescales, the southern processes could also contribute to the increasing of basin-scale N–S density contrast and the strengthening of the AMOC in LGM-2CO2. Both the reductions of meltwater in the north and brine rejection in the south are fully active at changing the density (see also the Appendix 2). However, it is difficult to separate their relative contributions because of the long timescale involved and the coupled nature of the system. In fact, the southern-induced increase of the AMOC could amplify itself by altering the northern processes, i.e., the increased northward heat transport can push the sea-ice edge further northward, causing a larger reduction of melting flux in the north and a stronger AMOC. A clear separation of them at centennial-millennial timescales would require additional sensitivity experiments, which is beyond the scope of this study.

Our results highlight the importance of sea-ice climatology and dynamics in determining the response and timescales of the AMOC (Yang and Neelin 1993; Lohmann and Gerdes 1998; Jayne and Marotzke 1999; Gildor and Tziperman 2003; Bitz et al. 2007; Banderas et al. 2012), especially under glacial conditions. At the LGM, the sea-ice formation (Fig. 12a, b, shading) and southward transport (vectors) are substantially greater than those in the modern climate, producing a significant melting centre in the mid-latitude. Doubling atmospheric CO_2 under glacial conditions could cause marked sea-ice retreat, which leads to less southward sea-ice export from the Arctic and the GIN Seas. The subsequent reduction of meltwater flux could strengthen the AMOC significantly. This is the far-field effect from sea-ice formation and transport (Stocker et al. 2001). Furthermore, in the Southern Ocean, the sea ice expands by almost 100 % at the LGM (Fig. 12c, d), which is also consistent with reconstructions from sediment cores (Gersonde et al. 2005). The expanded sea ice in the Southern Ocean at glacial time could also play an important role in modulating the AMOC at centennial-millennial timescales through the changes in brine rejection. Although there are still considerable uncertainties in the simulation of sea-ice processes in the current generation of coupled models (Flato et al. 2013), this work points out that in order to better simulate climate change—especially the abrupt changes related to the AMOC—it is essential to have a realistic representation of the sea-ice processes.

It is possible that processes identified in this study could be model or resolution dependent, especially considering the coarse resolution of our model, and the significant model bias (20 %) in simulating the Southern Ocean sea ice for the modern climate (Collins et al. 2006). Also, the poleward shift of the Southern Ocean westerlies in our

doubling CO_2 experiments (MOD-2CO2) is not as significant as the CMIP5 simulations (Swart and Fyfe 2012). However, it should be pointed out that the response of the AMOC for the modern climate–first a fast weakening and then a slow strengthening–is qualitatively consistent with the results from medium-resolution models (Bryan et al. 2006), the newer CCSM4 and CESM1 with improved physics (Meehl et al. 2012, 2013), and other CMIP5 models (Collins et al. 2013). Furthermore, the simulated hemispheric sea-ice extent and the glacial/interglacial changes (an order lager than the model bias) are coherent with the reconstructions from sediment cores (Sarnthein et al. 2003; Gersonde et al. 2005). These give us some confidence in our major findings.

Another possible limitation of this work is the lack of an interactive ice sheet model in CCSM3. The ice-sheet retreat could alter the behaviour of the AMOC through freshwater flux (Swingedouw et al. 2006; Hu et al. 2009) and possibly the reorganization of atmospheric circulations (Eisenman et al. 2009). As most of the "hosing experiments" (Stouffer et al. 2006; Hu et al. 2008; Brady and Otto-Bliesner 2011; Liu et al. 2013) show, after the termination of freshwater flux, the AMOC could recover toward its control strength in several hundreds of years when the excessive freshwater is removed from the hosing zone. Therefore, a moderate freshwater flux from the melting of the Laurentide and Greenland ice sheets may not change the final response of the AMOC to the CO_2 increase. However, the influences from the reorganization of atmospheric circulations could be permanent (Eisenman et al. 2009). We admit that in order to solve this problem directly, we have to incorporate an interactive ice sheet model, which surely deserves more study in the future.

Acknowledgments The authors thank Dr. Feng He for performing the transient experiments (TraCE-GHG) and Dr. Esther Brady for helpful comments that improved the quality of this paper. We gratefully acknowledge the constructive comments from two anonymous reviewers. This work is supported by the National Natural Science Foundation of China (NSFC 41130105), the Ministry of Science and Technology of China (MOST 2012CB955200), the U.S. National Science Foundation and the Department of Energy.

Appendix 1: A detailed heat and freshwater budget

To quantitatively evaluate the importance of different processes and feedbacks in changing the AMOC in doubling CO_2 experiments, we analyse the heat/freshwater budget for both the northern and southern box in the upper Atlantic Ocean. The time-varying equation for the volume-integrated heat/freshwater budget is

Table 3 Changes in the heat storage, surface flux and convergence of transport (units: 10^{-1} PW) in the northern (35°N–65°N) and southern box (0°N–30°N) in the upper North Atlantic Ocean in the doubling CO_2 experiments

		MOD-2CO2				LGM-2CO2			
		$\frac{dM_S}{dt}$	M_F	$-\mathrm{div}M_T$, $-\mathrm{div}M_{MOC}$, $-\mathrm{div}M_{az}$	R	$\frac{dM_S}{dt}$	M_F	$-\mathrm{div}M_T$, $-\mathrm{div}M_{MOC}$, $-\mathrm{div}M_{az}$	R
Initial (1–90 year)	Northern	**0.37**	**1.02**	−0.82	0.17	**0.39**	**1.29**	−1.06	0.16
				−1.71				−0.11	
				0.89				−0.95	
	Southern	**0.57**	−0.50	**0.61**	0.46	0.64	*−0.25*	*−0.12*	1.01
				0.99				*0.28*	
				−0.38				−0.16	
Intermediate (91–400 year)	Northern	0.07	*−0.17*	0.39	−0.15	**0.12**	**−0.50**	**0.59**	0.03
				0.37				2.23	
				0.02				−1.64	
	Southern	0.12	*−0.08*	*0.20*	0	0.02	0.35	−0.83	0.46
				−0.24				−1.75	
				0.44				0.92	
Final (401–1,500 year)	Northern	0.01	−0.33	0.48	−0.14	0.02	−0.25	0.47	−0.2
				0.59				0.78	
				−0.11				−0.31	
	Southern	0.01	*−0.03*	*−0.13*	*0.17*	0	*−0.05*	*−0.10*	0.15
				−0.40				−0.40	
				0.27				0.30	

The convergence of total heat transport is also separated into part by the AMOC and the azonal gyre transport. The residual term represents the heat transport by diffusion and convection. Numbers in italic are not significant at 95 % level. Important processes that relate to changes in the AMOC are highlighted in bold

$$\frac{dM_S}{dt} = M_F - \mathrm{div}M_T + R \quad (3)$$

where M_S is the heat/freshwater storage, M_F the area-integrated surface flux, $\mathrm{div}M_T$ divergence of the transport between the northern and southern boundary of the box, and R is the residual, including diffusion and convection with the lower ocean. The transport across certain latitude M_T can be further separated into the meridional part (M_{MOC}) and the azonal part (M_{az}). Take the freshwater transport as an example,

$$M_{MOC} = -\frac{1}{S_0}\int \overline{v}(z)\cdot\left(\langle\overline{S}\rangle - S_0\right)\cdot \mathrm{d}z \quad (4)$$

$$M_{az} = -\frac{1}{S_0}\int \overline{v(z)'\cdot S'}\cdot \mathrm{d}z \quad (5)$$

where the reference salinity S_0 is the averaged salinity of the Atlantic Ocean, 34.7 and 36.5 for the present day and the LGM, respectively. $\overline{v}(z)$ and $\langle\overline{S}\rangle$ denote the zonally integrated northward velocity and averaged salinity, and $v(z)'$ and S' represent the deviations from their zonal means.

The changes in heat storage, surface flux and convergence of transport in the northern and southern box during each stage are listed in Table 3. For both the MOD-2CO2 and LGM-2CO2, the increase of heat storage (0.04 PW) in the northern box during the initial weakening stage is mainly attributable to the increase of surface heat flux (0.10–0.13 PW). The convergence of heat transport is negative (−0.08 to −0.11 PW), indicating a negative feedback between the strength of the AMOC and heat transport. It works as follows: a weakening of the AMOC reduces the northward heat transport, leads to a cooling, and promotes the deep convection. It is interesting to note that during the intermediate strengthening stage in LGM-2CO2, the convergence of heat transport is positive (0.06 PW) because of the enhanced AMOC, and simultaneously the surface heat flux decreases significantly (−0.05 PW) due to the reduction of the sea-ice insulating effect and the increase of ocean temperature. The former, again, suggests a negative feedback between the AMOC and heat transport, while the latter indicates a positive feedback between the AMOC and the surface heat flux. This positive feedback can act through two different loops: Firstly, intensification in the AMOC transports more heat northward, leads to a warming and enhanced heat loss to the atmosphere. Secondly, a strengthening of the AMOC and heat transport can cause more sea-ice retreat and enhanced heat loss through the sea-ice insulating effect.

Table 4 Changes in the freshwater storage, surface flux and convergence of transport (10^{-1} Sv) in the northern (35°N–65°N) and southern box (0°N–30°N) in the upper North Atlantic Ocean in the doubling CO_2 experiments

		MOD-2CO2				LGM-2CO2			
		$\frac{dM_S}{dt}$	M_F	$-\mathrm{div}M_T$, $-\mathrm{div}M_{MOC}$, $-\mathrm{div}M_{az}$	R	$\frac{dM_S}{dt}$	M_F	$-\mathrm{div}M_T$, $-\mathrm{div}M_{MOC}$, $-\mathrm{div}M_{az}$	R
Initial (1–90 year)	Northern	−0.07	−0.21	0.73	0.59	0.02	−0.32	0.28	0.06
				1.18				−0.17	
				−0.45				0.45	
	Southern	−0.20	−0.34	*−0.10*	0.24	−0.46	−0.37	*−0.11*	0.02
				−0.91				*−0.03*	
				0.81				0.08	
Intermediate (91–400 year)	Northern	0	*−0.04*	*−0.02*	*0.06*	**−0.19**	**−0.58**	0.30	0.09
				−0.30				**−1.16**	
				0.28				**1.46**	
	Southern	−0.03	*−0.06*	*0.18*	*−0.15*	−0.04	*0.04*	0.21	−0.29
				0.21				1.57	
				−0.03				−1.36	
Final (401–1,500 year)	Northern	0	*−0.02*	*0.12*	*−0.10*	**−0.04**	**−0.26**	**−0.32**	0.62
				−0.57				**−0.68**	
				0.45				0.36	
	Southern	0	*−0.05*	*0.07*	*−0.02*	−0.04	−0.07	0.19	−0.16
				0.64				0.36	
				−0.57				−0.17	

The convergence of total heat transport is also separated into part by the AMOC and the azonal gyre transport. The residual term represents the heat transport by diffusion and convection. Numbers in italic are not significant at 95 % level. Important processes that relate to changes in the AMOC are highlighted in bold

The changes in freshwater storage, surface flux and convergence of transport in the northern and southern box during each stage are listed in Table 4. The most important process is the decrease of surface freshwater flux in the northern box (−0.06 Sv for the intermediate stage) caused by the reduction of meltwater flux (Fig. 11b). It could form a positive sea ice–ocean coupled feedback to intensify the AMOC. At the intermediate stage, the meridional part of freshwater transport (−0.12 Sv) acts to increase salinity in the northern box and stabilize the AMOC (a positive feedback) in LGM-2CO2; however, its role is overwhelmed by the azonal transport (0.15 Sv). The decrease of surface freshwater flux (−0.03 to −0.04 PW) in the southern box due to the enhanced evaporation in both climates during the initial weakening stage is another positive feedback, although overpowered by the negative feedback between the AMOC and surface heat flux.

Appendix 2: Confirmation from the EOF analysis

In order to confirm the crucial role of salinity changes in enhancing the N–S density contrast and, in turn, the intensification of the AMOC in LGM-2CO2, we use the empirical orthogonal function (EOF) analysis to detect the major modes of changes in zonal mean density, temperature and salinity in the doubling CO_2 experiments (Fig. 13). In MOD-2CO2, the EOF1 of zonal mean density (Fig. 13a) resembles the EOF1 of zonal mean temperature (Fig. 13d) very well with an N–S symmetric decrease of density, except for the northern polar region. This quasi-symmetric change of density agrees with insignificant changes in the AMOC at long timescales in MOD-2CO2. In sharp contrast, in LGM-2CO2, the evolution of the zonal mean density in the Atlantic Ocean is dominated by an N–S asymmetric mode (EOF1) with a significant increase of density in the upper 2,000 m and 40°S northward Atlantic Ocean and a comparable decrease in the deep and Southern Ocean (Fig. 13b). EOF1 can explain 92 % of the total variance and the corresponding PC1 (Fig. 13c) suggests that this mode has timescale longer than 1,000 years. This asymmetric mode can produce a stronger NADW and a weaker AABW through the increase of the N–S density contrast and the decrease of vertical stratification in the Atlantic Ocean, which is consistent with the strengthening of AMOC after the initial weakening in LGM-2CO2 (also shown in the initial stage of PC1). In order to find out, the relative

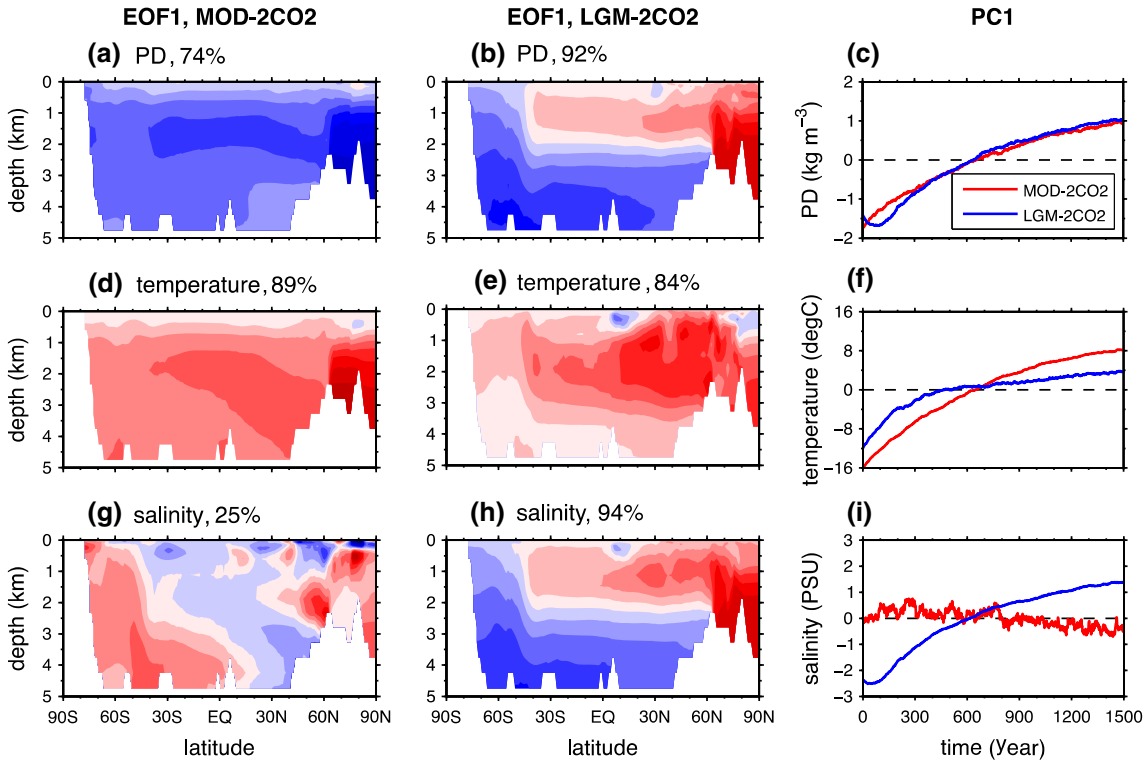

Fig. 13 First EOF of the Atlantic zonal mean potential density in the doubling CO_2 experiments for the modern climate (**a**) and LGM (**b**). The corresponding PCs for modern climate (*red*) and LGM (*blue*) are shown in **c**, **d**, **e** and **f** are the same, but for the zonal mean temperature, **g**, **h** and **i** are for the zonal mean salinity. All the EOFs are normalized, such that the magnitude is unit. The variance explained by the first EOF of the potential density, temperature and salinity are 74, 89 and 25 % for the modern climate, and 92, 84 and 94 % for LGM, respectively

contribution of the changes in temperature and salinity, we carry out the same EOF analysis for the zonal mean temperature and salinity in the Atlantic Ocean (Fig. 13e, h). The first EOF of temperature, which can explain 84 % of the total variance, shows the signal of global warming due to the doubling of CO_2. The warming in the upper and mid Atlantic Ocean is larger, which suggests the temperature change makes a negative contribution to the N–S density contrast. The first EOF of salinity, explaining 94 % of the total variance, resembles the asymmetric mode very well, indicating that the change of zonal mean salinity dominates the asymmetric change of zonal mean density in the Atlantic Ocean in LGM-2CO2.

The EOF analysis is coherent with the diagnosing of the trend of zonal mean potential density (Sects. 5.1–5.3) and confirms that the contribution from salinity changes plays the dominant role in increasing the N–S density contrast and strengthening the AMOC in LGM-2CO2 at centennial-millennial timescales. Therefore, we can exclude the role of Atlantic surface heat flux. Combining with the diagnose of the freshwater budget for the North Atlantic in Sect. 5.4, we could find, once again, that the reorganization of the Atlantic surface freshwater flux is of essential importance in strengthening the AMOC in LGM-2CO2. EOF analysis (Fig. 13h) also demonstrates that the increase of salinity in the north could be coupled with a decrease of salinity in the south at millennial timescale.

References

Banderas R, Ávarez-Solas J, Montoya M (2012) Role of CO2 and Southern Ocean winds in glacial abrupt climate change. Clim Past 8(3):1011–1021. doi:10.5194/cp-8-1011-2012

Bitz CM, Chiang JCH, Cheng W, Barsugli JJ (2007) Rates of thermohaline recovery from freshwater pulses in modern, last glacial maximum, and greenhouse warming climates. Geophys Res Lett 34(7):L07708. doi:10.1029/2006GL029237

Brady E, Otto-Bliesner B (2011) The role of meltwater-induced subsurface ocean warming in regulating the Atlantic meridional overturning in glacial climate simulations. Clim Dyn 37(7–8):1517–1532. doi:10.1007/s00382-010-0925-9

Bryan FO, Danabasoglu G, Nakashiki N, Yoshida Y, Kim D-H, Tsutsui J, Doney SC (2006) Response of the North Atlantic thermohaline circulation and ventilation to increasing carbon dioxide in CCSM3. J Clim 19(11):2382–2397. doi:10.1175/jcli3757.1

Bryan FO, Nakashiki N, Yoshida Y, Maruyama K (2007) Response of the meridional overturning circulation during differing pathways toward greenhouse gas stabilization. In: Ocean circulation: mechanisms and impacts—past and future changes of meridional overturning. American Geophysical Union, pp 351–363. doi:10.1029/173gm22

Collins WD, Bitz CM, Blackmon ML, Bonan GB, Bretherton CS, Carton JA, Chang P, Doney SC, Hack JJ, Henderson TB, Kiehl JT, Large WG, McKenna DS, Santer BD, Smith RD (2006) The community climate system model version 3 (CCSM3). J Clim 19(11):2122–2143. doi:10.1175/JCLI3761.1

Collins M, Knutti R, Arblaster J, Dufresne J-L, Fichefet T, Friedlingstein P, Gao X, Gutowski WJ, Johns T, Krinner G, Shongwe M, Tebaldi C, Weaver AJ, Wehner M (2013) Long-term climate change: projections, commitments and irreversibility. In: Stocker TF, Qin D, Plattner G-K, Tignor M, Allen SK, Boschung J, Nauels A, Xia Y, Bex V, Midgley PM (eds) Climate change 2013: the physical science basis. Contribution of Working Group I to the fifth assessment report of the intergovernmental panel on climate change. Cambridge University Press, Cambridge, pp 1029–1136

Danabasoglu G, Gent PR (2009) Equilibrium climate sensitivity: is it accurate to use a slab ocean model? J Clim 22(9):2494–2499. doi:10.1175/2008jcli2596.1

Duplessy JC, Shackleton NJ, Fairbanks RG, Labeyrie L, Oppo D, Kallel N (1988) Deepwater source variations during the last climatic cycle and their impact on the global deepwater circulation. Paleoceanography 3(3):343–360. doi:10.1029/PA003i003p00343

Eisenman I, Bitz CM, Tziperman E (2009) Rain driven by receding ice sheets as a cause of past climate change. Paleoceanography 24(4):PA4209. doi:10.1029/2009pa001778

Flato G, Marotzke J, Abiodun B, Braconnot P, Chou SC, Collins W, Cox P, Driouech F, Emori S, Eyring V, Forest C, Gleckler P, Guilyardi E, Jakob C, Kattsov V, Reason C, Rummukainen M (2013) Evaluation of climate models. In: Stocker TF, Qin D, Plattner G-K, Tignor M, Allen SK, Boschung J, Nauels A, Xia Y, Bex V, Midgley PM (eds) Climate change 2013: the physical science basis. Contribution of Working Group I to the Fifth Assessment Report of the Intergovernmental Panel on Climate Change. Cambridge University Press, Cambridge, pp 741–866

Ganachaud A, Wunsch C (2000) Improved estimates of global ocean circulation, heat transport and mixing from hydrographic data. Nature 408(6811):453–457. doi:10.1038/35044048

Gersonde R, Crosta X, Abelmann A, Armand L (2005) Sea-surface temperature and sea ice distribution of the Southern Ocean at the EPILOG last glacial maximum—a circum-Antarctic view based on siliceous microfossil records. Quat Sci Rev 24(7–9):869–896. doi:10.1016/j.quascirev.2004.07.015

Gildor H, Tziperman E (2003) Sea-ice switches and abrupt climate change. Philos Trans R Soc Lond Ser A Math Phys Eng Sci 361(1810):1935–1944. doi:10.1098/rsta.2003.1244

Gregory JM, Dixon KW, Stouffer RJ, Weaver AJ, Driesschaert E, Eby M, Fichefet T, Hasumi H, Hu A, Jungclaus JH, Kamenkovich IV, Levermann A, Montoya M, Murakami S, Nawrath S, Oka A, Sokolov AP, Thorpe RB (2005) A model intercomparison of changes in the Atlantic thermohaline circulation in response to increasing atmospheric CO2 concentration. Geophys Res Lett 32(12):L12703. doi:10.1029/2005gl023209

He F (2011) Simulating transient climate evolution of the last deglaciation with CCSM3. Dissertation, University of Wisconsin-Madison, Madison, USA

He F, Shakun JD, Clark PU, Carlson AE, Liu Z, Otto-Bliesner BL, Kutzbach JE (2013) Northern Hemisphere forcing of Southern Hemisphere climate during the last deglaciation. Nature 494(7435):81–85. doi:10.1038/nature11822

Hieronymus M, Nycander J (2012) The buoyancy budget with a nonlinear equation of state. J Phys Oceanogr 43(1):176–186. doi:10.1175/JPO-D-12-063.1

Hu A, Otto-Bliesner BL, Meehl GA, Han W, Morrill C, Brady EC, Briegleb B (2008) Response of thermohaline circulation to freshwater forcing under present-day and LGM Conditions. J Clim 21(10):2239–2258. doi:10.1175/2007jcli1985.1

Hu A, Meehl GA, Han W, Yin J (2009) Transient response of the MOC and climate to potential melting of the Greenland ice sheet in the 21st century. Geophys Res Lett 36(10):L10707. doi:10.1029/2009gl037998

Jayne SR, Marotzke J (1999) A destabilizing thermohaline circulation-atmosphere-sea ice feedback. J Clim 12(2):642–651. doi:10.1175/1520-0442(1999)012<0642:adtcas>2.0.co;2

Klocker A, McDougall TJ (2010) Influence of the nonlinear equation of state on global estimates of dianeutral advection and diffusion. J Phys Oceanogr 40(8):1690–1709. doi:10.1175/2010JPO4303.1

Knorr G, Lohmann G (2007) Rapid transitions in the Atlantic thermohaline circulation triggered by global warming and meltwater during the last deglaciation. Geochem Geophys Geosyst 8(12):Q12006. doi:10.1029/2007gc001604

Kutzbach JE, He F, Vavrus SJ, Ruddiman WF (2013) The dependence of equilibrium climate sensitivity on climate state: applications to studies of climates colder than present. Geophys Res Lett 40(14):3721–3726. doi:10.1002/grl.50724

Liu Z (2006) Glacial thermohaline circulation and climate: forcing from the north or south? Adv Atmos Sci 23(2):199–206. doi:10.1007/s00376-006-0199-7

Liu Z, Shin S-I, Webb RS, Lewis W, Otto-Bliesner BL (2005) Atmospheric CO2 forcing on glacial thermohaline circulation and climate. Geophys Res Lett 32(2):L02706. doi:10.1029/2004gl021929

Liu Z, Otto-Bliesner BL, He F, Brady EC, Tomas R, Clark PU, Carlson AE, Lynch-Stieglitz J, Curry W, Brook E, Erickson D, Jacob R, Kutzbach J, Cheng J (2009) Transient simulation of last deglaciation with a new mechanism for Bølling-Allerød warming. Science 325(5938):310–314. doi:10.1126/science.1171041

Liu W, Liu Z, Hu A (2013) The stability of an evolving Atlantic meridional overturning circulation. Geophys Res Lett 40(8):1562–1568. doi:10.1002/grl.50365

Lohmann G, Gerdes RD (1998) Sea ice effects on the sensitivity of the thermohaline circulation. J Clim 11(11):2789–2803. doi:10.1175/1520-0442(1998)011<2789:sieots>2.0.co;2

Lynch-Stieglitz J, Adkins JF, Curry WB, Dokken T, Hall IR, Herguera JC, Hirschi JJ, Ivanova EV, Kissel C, Marchal O, Marchitto TM, McCave IN, McManus JF, Mulitza S, Ninnemann U, Peeters F, Yu E-F, Zahn R (2007) Atlantic meridional overturning circulation during the last glacial maximum. Science 316(5821):66–69. doi:10.1126/science.1137127

McManus JF, Francois R, Gherardi JM, Keigwin LD, Brown-Leger S (2004) Collapse and rapid resumption of Atlantic meridional circulation linked to deglacial climate changes. Nature 428(6985):834–837. doi:10.1038/nature02494

Meehl GA, Washington WM, Arblaster JM, Hu A, Teng H, Tebaldi C, Sanderson BN, Lamarque J-F, Conley A, Strand WG, White JB (2012) Climate system response to external forcings and climate change projections in CCSM4. J Clim 25(11):3661–3683. doi:10.1175/JCLI-D-11-00240.1

Meehl GA, Washington WM, Arblaster JM, Hu A, Teng H, Kay JE, Gettelman A, Lawrence DM, Sanderson BM, Strand WG (2013) Climate change projections in CESM1(CAM5) compared to CCSM4. J Clim 26(17):6287–6308. doi:10.1175/JCLI-D-12-00572.1

Oka A, Hasumi H, Abe-Ouchi A (2012) The thermal threshold of the Atlantic meridional overturning circulation and its control by wind stress forcing during glacial climate. Geophys Res Lett 39(9):L09709. doi:10.1029/2012gl051421

Otto-Bliesner BL, Hewitt CD, Marchitto TM, Brady E, Abe-Ouchi A, Crucifix M, Murakami S, Weber SL (2007) Last glacial maximum ocean thermohaline circulation: PMIP2 model intercomparisons and data constraints. Geophys Res Lett 34(12):L12706. doi:10.1029/2007GL029475

Peltier WR (2004) Global glacial isostasy and the surface of the ice-age earth: the ICE-5G (VM2) model and grace. Annu Rev Earth Planet Sci 32(1):111–149. doi:10.1146/annurev.earth.32.082503.144359

Rahmstorf S, Ganopolski A (1999) Long-term global warming scenarios computed with an efficient coupled climate model. Clim Change 43(2):353–367. doi:10.1023/a:1005474526406

Robinson LF, Adkins JF, Keigwin LD, Southon J, Fernandez DP, Wang S-L, Scheirer DS (2005) Radiocarbon variability in the Western North Atlantic during the last deglaciation. Science 310(5753):1469–1473. doi:10.1126/science.1114832

Saenko OA, Eby M, Weaver AJ (2004) The effect of sea-ice extent in the North Atlantic on the stability of the thermohaline circulation in global warming experiments. Clim Dyn 22(6–7):689–699. doi:10.1007/s00382-004-0414-0

Sarnthein M, Pflaumann U, Weinelt M (2003) Past extent of sea ice in the northern North Atlantic inferred from foraminiferal paleotemperature estimates. Paleoceanography 18(2):1047. doi:10.1029/2002PA000771

Schmitt RW, Bogden PS, Dorman CE (1989) Evaporation minus precipitation and density fluxes for the North Atlantic. J Phys Oceanogr 19(9):1208–1221. doi:10.1175/1520-0485(1989)019<1208:empadf>2.0.co;2

Schmittner A, Latif M, Schneider B (2005) Model projections of the North Atlantic thermohaline circulation for the 21st century assessed by observations. Geophys Res Lett 32(23):L23710. doi:10.1029/2005gl024368

Shin S-I, Liu Z, Otto-Bliesner BL, Kutzbach JE, Vavrus SJ (2003a) Southern Ocean sea-ice control of the glacial North Atlantic thermohaline circulation. Geophys Res Lett 30(2):1096. doi:10.1029/2002gl015513

Shin SI, Liu Z, Otto-Bliesner B, Brady E, Kutzbach J, Harrison S (2003b) A simulation of the last glacial maximum climate using the NCAR-CCSM. Clim Dyn 20(2–3):127–151. doi:10.1007/s00382-002-0260-x

Speer K, Tziperman E (1992) Rates of water mass formation in the North Atlantic Ocean. J Phys Oceanogr 22(1):93–104. doi:10.1175/1520-0485(1992)022<0093:ROWMFI>2.0.CO;2

Stocker TF, Knutti R, Plattner GK (2001) The future of the thermohaline circulation—a perspective. In: The oceans and rapid climate change: past, present, and future, vol 126. Geophys. Monogr. Ser. AGU, Washington, DC, pp 277–293. doi:10.1029/GM126p0277

Stouffer RJ (2004) Time scales of climate response. J Clim 17(1):209–217. doi:10.1175/1520-0442(2004)017<0209:tsocr>2.0.co;2

Stouffer RJ, Manabe S (2003) Equilibrium response of thermohaline circulation to large changes in atmospheric CO2 concentration. Clim Dyn 20(7–8):759–773. doi:10.1007/s00382-002-0302-4

Stouffer RJ, Yin J, Gregory JM, Dixon KW, Spelman MJ, Hurlin W, Weaver AJ, Eby M, Flato GM, Hasumi H, Hu A, Jungclaus JH, Kamenkovich IV, Levermann A, Montoya M, Murakami S, Nawrath S, Oka A, Peltier WR, Robitaille DY, Sokolov A, Vettoretti G, Weber SL (2006) Investigating the causes of the response of the thermohaline circulation to past and future climate changes. J Clim 19(8):1365–1387. doi:10.1175/jcli3689.1

Swart NC, Fyfe JC (2012) Observed and simulated changes in the Southern Hemisphere surface westerly wind-stress. Geophys Res Lett 39(16):L16711. doi:10.1029/2012GL052810

Swingedouw D, Braconnot P, Marti O (2006) Sensitivity of the Atlantic meridional overturning circulation to the melting from northern glaciers in climate change experiments. Geophys Res Lett 33(7):L07711. doi:10.1029/2006gl025765

Swingedouw D, Braconnot P, Delecluse P, Guilyardi E, Marti O (2007) Quantifying the AMOC feedbacks during a 2×CO2 stabilization experiment with land-ice melting. Clim Dyn 29(5):521–534. doi:10.1007/s00382-007-0250-0

Talley LD, Reid JL, Robbins PE (2003) Data-based meridional overturning stream functions for the global ocean. J Clim

16(19):3213–3226. doi:10.1175/1520-0442(2003)016<3213:dmosft>2.0.co;2

Toggweiler JR, Russell J (2008) Ocean circulation in a warming climate. Nature 451(7176):286–288. doi:10.1038/nature06590

Voss R, Mikolajewicz U (2001) Long-term climate changes due to increased CO2 concentration in the coupled atmosphere-ocean general circulation model ECHAM3/LSG. Clim Dyn 17(1):45–60. doi:10.1007/pl00007925

Weaver AJ, Eby M, Kienast M, Saenko OA (2007) Response of the Atlantic meridional overturning circulation to increasing atmospheric CO2: sensitivity to mean climate state. Geophys Res Lett 34(5):L05708. doi:10.1029/2006gl028756

Weaver AJ, Sedláček J, Eby M, Alexander K, Crespin E, Fichefet T, Philippon-Berthier G, Joos F, Kawamiya M, Matsumoto K, Steinacher M, Tachiiri K, Tokos K, Yoshimori M, Zickfeld K (2012) Stability of the Atlantic meridional overturning circulation: a model intercomparison. Geophys Res Lett 39(20):L20709. doi:10.1029/2012gl053763

Wood RA, Vellinga M, Thorpe R (2003) Global warming and thermohaline circulation stability. Philos Trans R Soc Lond Ser A Math Phys Eng Sci 361(1810):1961–1975. doi:10.1098/rsta.2003.1245

Yang J, Neelin JD (1993) Sea–ice interaction with the thermohaline circulation. Geophys Res Lett 20(3):217–220. doi:10.1029/92GL02920

Yang H, Zhu J (2011) Equilibrium thermal response timescale of global oceans. Geophys Res Lett 38(14):L14711. doi:10.1029/2011gl048076

Yeager SG, Shields CA, Large WG, Hack JJ (2006) The low-resolution CCSM3. J Clim 19(11):2545–2566. doi:10.1175/jcli3744.1